ill-posed DOT image reconstruction problem. This same approach has been investigated extensively for EEG and MEG techniques; registration to an anatomical MRI image can be used to restrain the source reconstruction problem and has been shown to be of significant benefit (Dale and Sereno, 1993; Huppertz et al., 1998). The same has been achieved for diffuse optical tomography using subject-specific MRI images (Barbour et al., 1995; Boas and Dale, 2005; Ntziachristos et al., 2002). However, the requirement to obtain a subject's MRI undermines one of the fundamental advantages of DOT systems: that they are portable and can be easily applied to vulnerable subjects. A promising alternative is therefore to use a registered 3D atlas head model in place of the subject's MRI, as described by Custo et al. (2010). This MRI-free approach to anatomically guided DOT image reconstruction and interpretation is based on registering a selected atlas to the subject's head surface and solving the photon migration forward problem in the registered atlas space. This approach requires measuring the positions of the optical sources and detectors and the cranial landmarks of the subject's head in 3D space, commonly using an electromagnetic tracking system. This allows the atlas to be transformed into the subject space (or 'registered') using an affine transformation computed using the corresponding cranial landmarks in the two spaces (Singh et al., 2005; Tsuzuki et al., 2007).

Atlas-guided DOT will clearly exhibit errors in the localization of cortical activations. The sources of this error will be: 1) imperfect registration between the subject and atlas spaces, 2) differences between the subject's true anatomy and the atlas anatomy and 3) the localization error associated with diffuse optical image reconstruction. These sources of error have previously been investigated, but not in combination. Studies have shown that by employing the subject-specific MRI, the error associated with DOT localization of simulated brain activation in the cortex is 5–10 mm (Boas and Dale, 2005). The error due to the registration process has also been explicitly investigated and found to be on the order of 4–7 mm (Singh et al., 2005; Tsuzuki et al., 2007). However, it is clearly necessary to explicitly test the entire atlas-based DOT process, and how errors in localization, registration and anatomy will affect the accuracy of the image reconstruction process.

In this paper we seek to validate the atlas-guided DOT methods described in Custo et al. (2010), and quantify the corresponding error in the localization of simulated cortical activations. Using an MRI library of 32 subjects, we simulate DOT measurements of brain activation in the subject space then reconstruct the corresponding DOT images using both an atlas registered to the subject and the subject's true anatomy. This allows us to directly compare the anatomical location of the images reconstructed in the atlas space with those reconstructed in the subject space.

Materials and methods

MRI data, atlas and pre-processing

Anatomical MRI images with a voxel size of $0.94\times0.94\times1.5$ mm were obtained using the multi-echo FLASH pulse sequence described in Fischl et al. (2004) for 32 adult subjects. The atlas MRI volume we employed was the high-resolution 'Colin27' digital brain phantom as described by Collins et al. (1998). The atlas MRI volume and all subject MRI volumes were automatically transformed into a single coordinate system in FreeSurfer, which ensures consistent orientation. Preprocessing of the 32 individual MRI volumes and of the anatomical MRI atlas was performed in order to segment the volumes and extract the pia mater surface as a 3D mesh. The subject-specific MRI volumes were segmented into gray matter, white matter and extra-cerebral tissue, using FreeSurfer (http://surfer.nmr.mgh.harvard.edu) (Dale et al., 1999; Fischl et al., 1999). The anatomical atlas was segmented in the same manner and then registered to each subject space using an affine transformation from the 10/20 scalp positions on the atlas to the 10/20 scalp positions on the real anatomy (Singh et al., 2005). The 10/20 scalp positions were identified on the different head surfaces following the procedure outlined in Jurcak et al. (2007). This pre-processing produced 32 segmented subject brain volumes and 32 registered, segmented atlas volumes.

Virtual DOT probe and sensitivity mapping

In order to simulate DOT measurements it was first necessary to produce a virtual DOT probe and map this probe to our 32 MRI data sets and our 32 registered atlases. We utilized a large virtual probe with 100 detectors and 29 sources arranged in a hexagonal pattern such that the nearest and second-nearest source-detector separations are 20 and 34.6 mm respectively. The virtual probe was created in 2D space, but was designed to be wrapped to the 3D surface of the scalp. The 2D probe was first anchored in each MRI space such that the midline of the probe was aligned to the midline of each head (i.e. the nasion–inion sagittal plane) and a specific optode was positioned at Cz, the apex of the head. The remaining 128 source and detector positions were then wrapped to the head using an iterative, spring-relaxation algorithm. This algorithm introduces a spring constant between nearest neighbor optodes such that a force is applied if the separation between those optodes deviates from the optimal 20 mm. The force exerted on the optodes was then minimized by allowing the optodes to move in 3D space by up to 1 mm per iteration. Between iterations, all optode locations are forced to the surface of the scalp. Iterations continued until optode locations converged. After this process was complete, the average nearest and second-nearest source-detector separations, were 20.1 ($\pm$0.69) and 34.5 ($\pm$0.91) mm. The 2D probe is shown in Fig. 1a, and the virtual probe wrapped to a registered atlas head is shown in Figs. 1b and c. Note that in a real atlas-based DOT study, the 3D coordinates of the optode positions on the subject scalp would be measured and those positions would then be transformed into the registered atlas space. For the current study, we wrapped the virtual probe to the registered atlas directly rather than transforming the subject-space optode positions. The transformation of optode locations usually results in many optodes being placed above or below the scalp, which then necessitates the application of a relaxation algorithm similar to that described above to force the optodes to the scalp and correct source–detector separations.

Once we had obtained each source and detector position for each of the 64 head models, Monte Carlo photon migration simulations were performed using a GPU-based Monte Carlo algorithm (Fang, 2010). Measurement sensitivity profiles were obtained for the nearest and second-nearest neighbor source–detector pairs, providing a total of 284 channels. The absorption and reduced scattering coefficients were 0.0178 mm^{-1} and 1.25 mm^{-1} for white matter and gray matter and 0.0159 mm^{-1} and 0.8 mm^{-1} for extra-cerebral tissues respectively (Boas and Dale, 2005). The resulting measurement sensitivity profiles form rows in the matrix $\boldsymbol{A}$ that transforms from the voxel space of localized changes in the absorption coefficient, $\boldsymbol{x}$, to the measurement space $\boldsymbol{y}$ of optical density changes. That is, $\boldsymbol{y}=\boldsymbol{A}\,\boldsymbol{x}$. Summing along columns of $\boldsymbol{A}$, we obtain the aggregate sensitivity of our probe geometry to absorption changes at each voxel. This aggregate sensitivity to absorption changes within the cortex is exemplified for three subjects in Fig. 2.

Simulating cortical activation

Given the measurement sensitivity matrix, simulated DOT measurements of brain activation can be computed by first simulating a vector which defines a change in the absorption coefficient of selected voxels. Simulating an activation in the subject space allows us to compute the localization errors inherent to the DOT images reconstructed using both the subject's anatomy and the atlas anatomy.

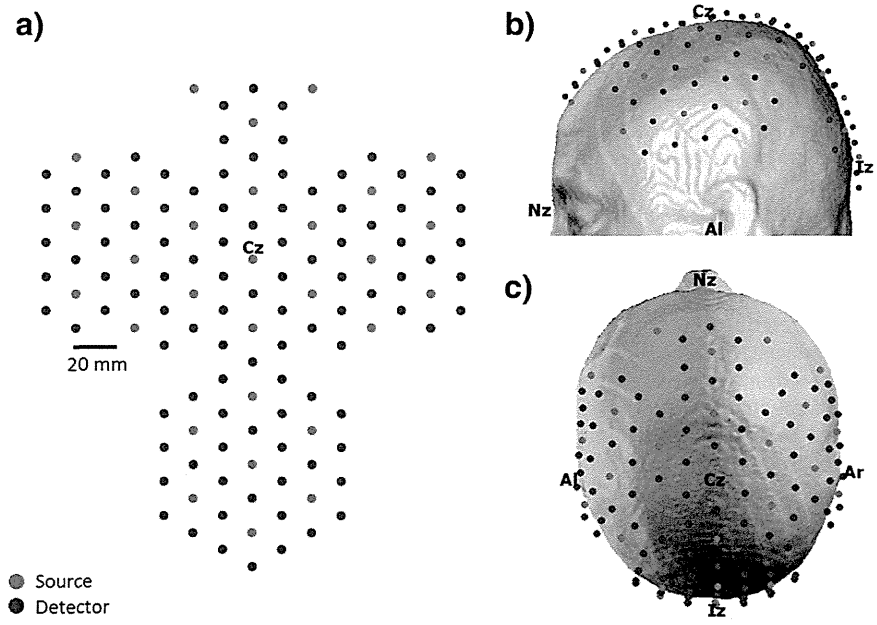

Fig. 1. The virtual probe layout is shown in 2D (a) and wrapped to the atlas head in (b) and (c). The anchor point Cz is shown as the 10–20 landmarks. This probe layout includes source–detector separations of 20 mm and 34.6 mm.

In order to quantify the localization error as a function of cortical position, we simulated approximately 4000 individual brain activations across the cortex in each of the 32 subject MRI spaces. Each simulated brain activation was centered on a unique voxel in the segmented cortex of the subject's MRI. The position of each brain activation was made anatomically equivalent across all 32 subjects using the surface transformation approach described below. The positions of the simulated activations were chosen primarily to provide good spatial coverage of the cortex across all subjects. The center of each simulated activation was displaced by at least 4 mm from neighboring activations, while regions of poor sensitivity (less than 1% of the maximum sensitivity in each subject) were avoided where possible. In some cases (particularly towards the edges of the virtual probe) activations had to be simulated in regions of low sensitivity in order to maintain coverage. Once the center of the activation had been determined, an iterative diffusion process was applied so that the magnitude of the activation absorption change decreased with distance from the center and reached zero at 10 mm from the center in all directions. The volume of each activation was restricted to the segmented gray matter. Examples of five different brain activations produced in 3 different subjects at anatomically equivalent locations are shown in Fig. 3.

Given the measurement sensitivity matrix ($\boldsymbol{A}$) and the simulated vector of brain activations in each subject space ($\boldsymbol{x}_{\mathbf{truth,subject}}$), we were then able to calculate the simulated DOT measurement vector via: $\boldsymbol{y} = \boldsymbol{A}_{\mathbf{subject}}\, \boldsymbol{x}_{\mathbf{truth,subject}}$.

Image reconstruction

Using the DOT measurements simulated in each of the 32 subjects, we were able to reconstruct DOT images of brain activation for each of the 32 subject and 32 registered atlas volumes. As described by Arridge (1999), and Boas and Dale (2005) this constitutes solving the inverse problem:

$$x = A^{\mathrm{T}}\left(AA^{\mathrm{T}} + \lambda\sigma_y^2\right)^{-1} y \tag{1}$$

where σ_y^2 is the measurement covariance matrix (assumed to be diagonal) and $\lambda = \alpha * \max(\mathrm{diag}(\boldsymbol{A}\boldsymbol{A}^{\mathrm{T}}))$ is the scalar regularization parameter. We set $\alpha = 0.01$, which is consistent with previous simulated and in-vivo diffuse optical reconstruction studies where NIRS measurements are expected to have a standard deviation of ~1%, which is typical for source–detector separations of ~3 cm (Boas and

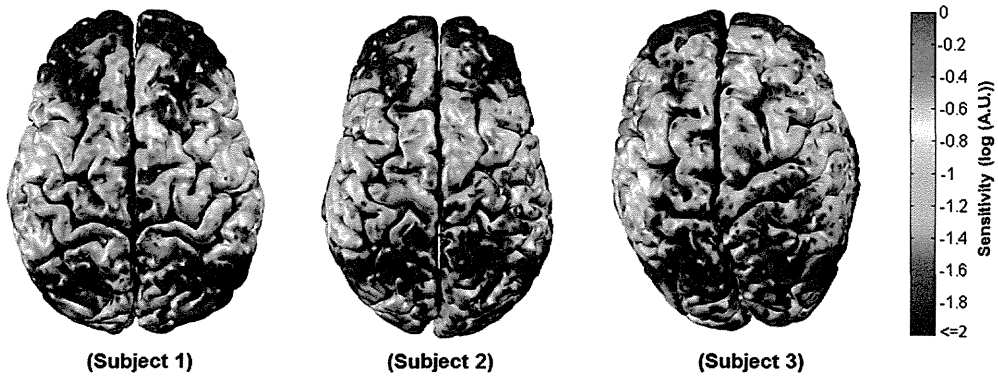

Fig. 2. The normalized cortical sensitivity of the virtual NIRS probe in three subjects. Areas where the probe is sparse, such as over the lateral frontal lobes, clearly exhibit a reduced sensitivity. Note that all sensitivities below 1% of the subject maximum are shown in dark blue.

Fig. 3. Five simulated activations in their anatomically equivalent locations in three subjects.

Dale, 2005; Custo et al., 2010). No noise was added to the simulated measurements as we wished to focus on the localization errors of atlas-guided DOT rather than exploring the impact of noise. The sensitivity matrix, $\boldsymbol{A}$, used in this image reconstruction was either that of a given subject, $\boldsymbol{A}_{\mathbf{subject}}$, or that of a registered atlas, $\boldsymbol{A}_{\mathbf{atlas}}$. In both cases, the reconstruction was constrained to cortical voxels only. The application of this constraint has been shown in previous simulations to significantly increase the accuracy of optical reconstructions, which, without such a constraint, have a strong tendency to underestimate the depth of a given activation (see Boas and Dale, 2005). These image reconstruction processes resulted in ~4000 DOT images of simulated cortical activation for each of the 32 subject volumes and each of the 32 registered atlas volumes. Images computed using the subjects' true anatomy are denoted as $\boldsymbol{x}_{\mathbf{recon,subject}}$, whereas those computed using the registered atlas are denoted as $\boldsymbol{x}_{\mathbf{recon,atlas}}$.

Error computation

In order to calculate the localization error of the brain activation reconstructed using each atlas, it was first necessary to transform the simulated activation location from the subject to the registered atlas space. That is, we need to find $\boldsymbol{x}_{\mathbf{truth,atlas}}$ given $\boldsymbol{x}_{\mathbf{truth,subject}}$. FreeSurfer (http://surfer.nmr.mgh.harvard.edu) provides an appropriate approach to locate anatomically corresponding locations in two different brains (Dale et al., 1999; Fischl et al., 1999). For each brain hemisphere the surface between the gray matter and the extra-cerebral tissues is calculated (i.e. the pial surface). This surface is then transformed, through a virtual inflation process, into a unitary sphere (each brain hemisphere surface is topologically equivalent to a sphere) while maintaining information about the folding pattern of the hemisphere. Different unitary spheres then lie in a common unitary space and their folding patterns are warped to a common template. Each of these transformation steps is reversible such that it is possible to transform from a point on the cortex of one brain to a point on the cortex of another to find common anatomical locations on two different brains. This enabled us to obtain $\boldsymbol{x}_{\mathbf{truth,atlas}}$ given $\boldsymbol{x}_{\mathbf{truth,subject}}$.

For each activation location, we calculated error metrics to characterize the distance between the true and reconstructed activation locations, for the 32 registered atlases ($\boldsymbol{x}_{\mathbf{recon,atlas}}$ vs. $\boldsymbol{x}_{\mathbf{truth,atlas}}$) and the 32 subject volumes ($\boldsymbol{x}_{\mathbf{recon,subject}}$ vs. $\boldsymbol{x}_{\mathbf{truth,subject}}$). To define the location of activation in the reconstructed DOT images, we first selected all voxels exhibiting an absorption change greater than 80% of the maximum absorption change in each image. The centroid of the reconstructed activation was then calculated by taking an absorption-change-weighted average of the position of these selected voxels. Three different localization error metrics were then computed:

Euclidean distance (volume): the distance in 3D space between the centroid of reconstructed activation and the centroid of the simulated activation.

Geodesic distance (surface): the shortest distance along the cortical surface between the centroids of the reconstructed and simulated activations. This is informative when two activations are close to each other but lie on different cortical folds. In this case the Euclidean error would be small despite the reconstructed activation being in the wrong cortical area. In such situations the geodesic distance provides a more informative measure of localization error.

Hausdorff distance (Hausdorff): defined as the length of the greatest local deviation between the two sets of points (Huttenlocher et al., 1993). The Hausdorff distance measures the deformation of the reconstructed activation profile relative to the simulated activation profile. The activation profiles are defined in the same way for both reconstructed and simulated activations: by selecting voxels which exceed 80% of the maximum absorption change in each image. The Hausdorff distance provides a measure of how accurately a DOT image maintains the shape of a simulated activation, rather than simply the location of its centroid. The Hausdorff error can be non-zero even if the reconstructed and simulated activation profiles are centered at a common voxel.

As described above, the error in localization inherent to atlas-guided DOT has three distinct sources. The error associated with diffuse optical image reconstruction is compounded by errors in atlas registration and anatomical differences between the subject and atlas. Any error in the registration of the atlas to the subject space, calculated via the 10–20 cranial landmarks, will produce an error in the positioning of the virtual DOT optodes. That is, the optode positioning error is a function of registration error. The optode positioning error will be inherent to the Euclidean, geodesic and Hausdorff metrics described above. However, in order to show that positioning of our simulated NIRS probe does not impact the localization errors, we explicitly calculated the optode positioning error by comparing the positions of each of the simulated optodes between every subject and subject-registered atlas. The distance between each optode and the three nearest 10-20 positions was calculated in both the registered atlas and subject spaces. These three distances describe a unique position in 3D space. The error in optode positioning was then calculated by taking the mean of the absolute difference between each distance in atlas space and its subject-space equivalent.

A diagram showing the whole data processing stream employed in this study, including registration, sensitivity mapping, simulating

brain activations, image reconstruction and error computation is shown in Fig. 4.

Results

The optode positioning error was calculated for each of the 32 registered atlas heads, and the average for each optode position is depicted in Fig. 5. Note that the largest errors occur where the head surface is highly curved, particularly towards the occipital region. The average (and standard deviation) optode positioning error across all subjects and optodes was 2.8 ($\pm$1.7) mm.

Fig. 6 shows seven simulated activations, but in addition shows the corresponding DOT images reconstructed using the subject-specific anatomy (Fig. 6b) and the atlas anatomy (Fig. 6c) for one subject. This result is characteristic of those across the data set, and clearly shows that reasonable, but decreased localization accuracy is associated with atlas-based reconstruction. Note that as we are interested in the location, rather than the scale of the reconstructed activation, each image is scaled to its own maximum absorption change.

Using the reconstructed DOT images of the ~4000 simulated activations and a process of interpolation, it was possible to calculate the Euclidean, geodesic and Hausdorff error metrics at nearly every point on the cortex for each of the 32 subject and 32 registered atlas heads. The error value assigned to each voxel is a weighted sum of the localization error of every activation center within 5 mm of that voxel. If there are less than 3 activation centers within 5 mm, no error value is assigned to that voxel (such voxels appear gray in Figs. 7 and 8). This process produced a near-continuous cortical map of localization error for each metric and each brain. These error maps can be displayed in either the subject or atlas space using the reversible FreeSurfer anatomical transformation described above. By averaging the error associated with each of the ~4000 activations across all 32 subjects, transforming to the atlas space and then repeating our interpolation process, we are able to produce maps of mean localization error.

Fig. 7 shows examples of the Euclidean, geodesic and Hausdorff localization error maps, for atlas-guided DOT processing in three subjects. The spatial pattern of each error metric is expected to differ

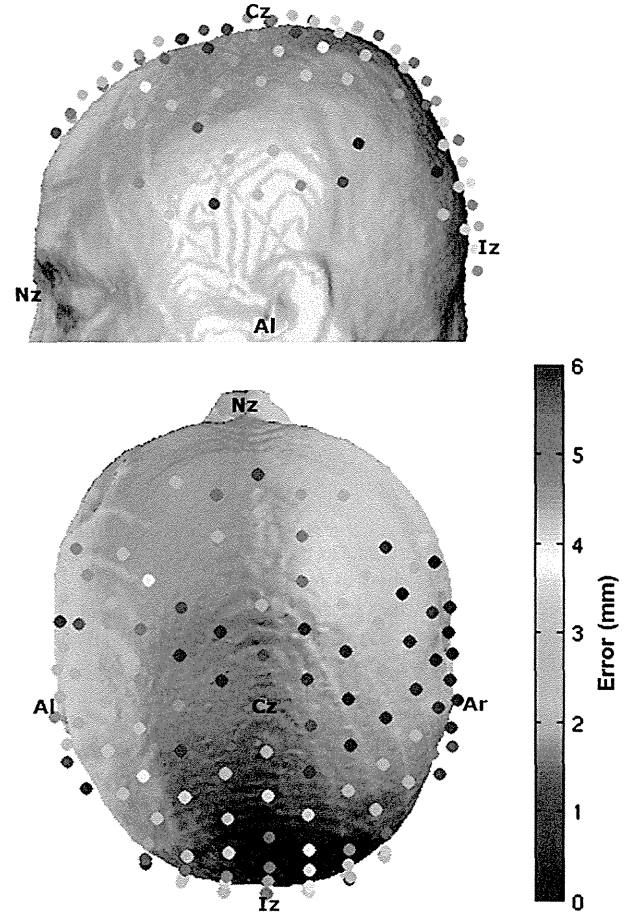

Fig. 5. The average error in optode positioning between subject and registered atlas.

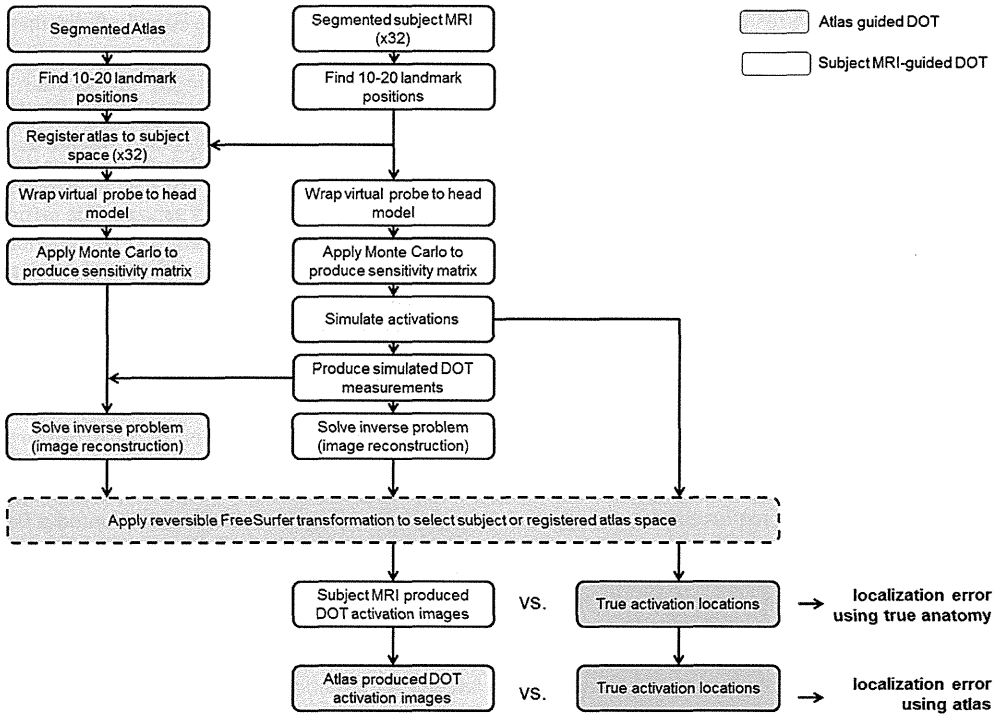

Fig. 4. A flow diagram illustrating every stage of analysis.

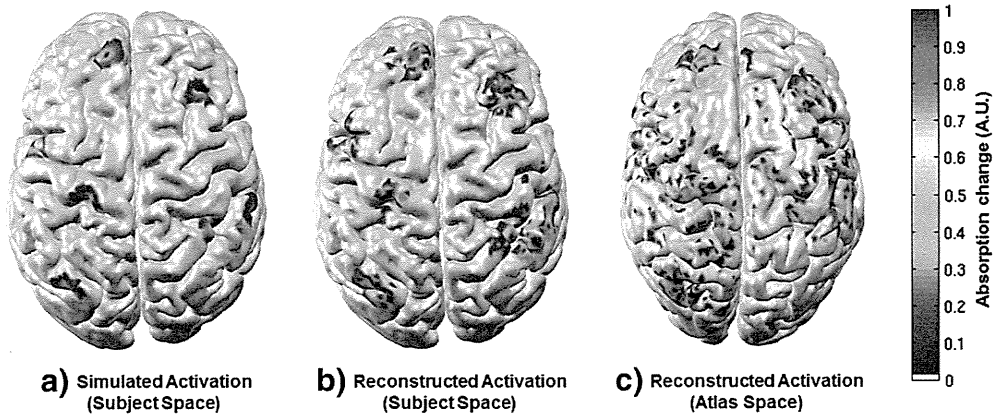

Fig. 6. Seven activations are shown as simulated in the subject space (a), reconstructed in the subject space (b) and reconstructed in the atlas space (c). Each figure is normalized by its own maximum absorption change.

from subject to subject because of anatomical variation, and the location of the largest error varies significantly from subject to subject. Note that in each subject the geodesic distance is generally greater than the Euclidean distance. Fig. 8 shows the average of the three localization error metrics across the 32 subjects for both atlas-guided and subject-MRI guided DOT processing. The geodesic error is consistently larger than the Euclidean error, for both forms of DOT processing. The Hausdorff distance is comparable to the Euclidean distance in regions of high localization error, but is generally higher than the Euclidean distance in regions of low error. The mean of each error

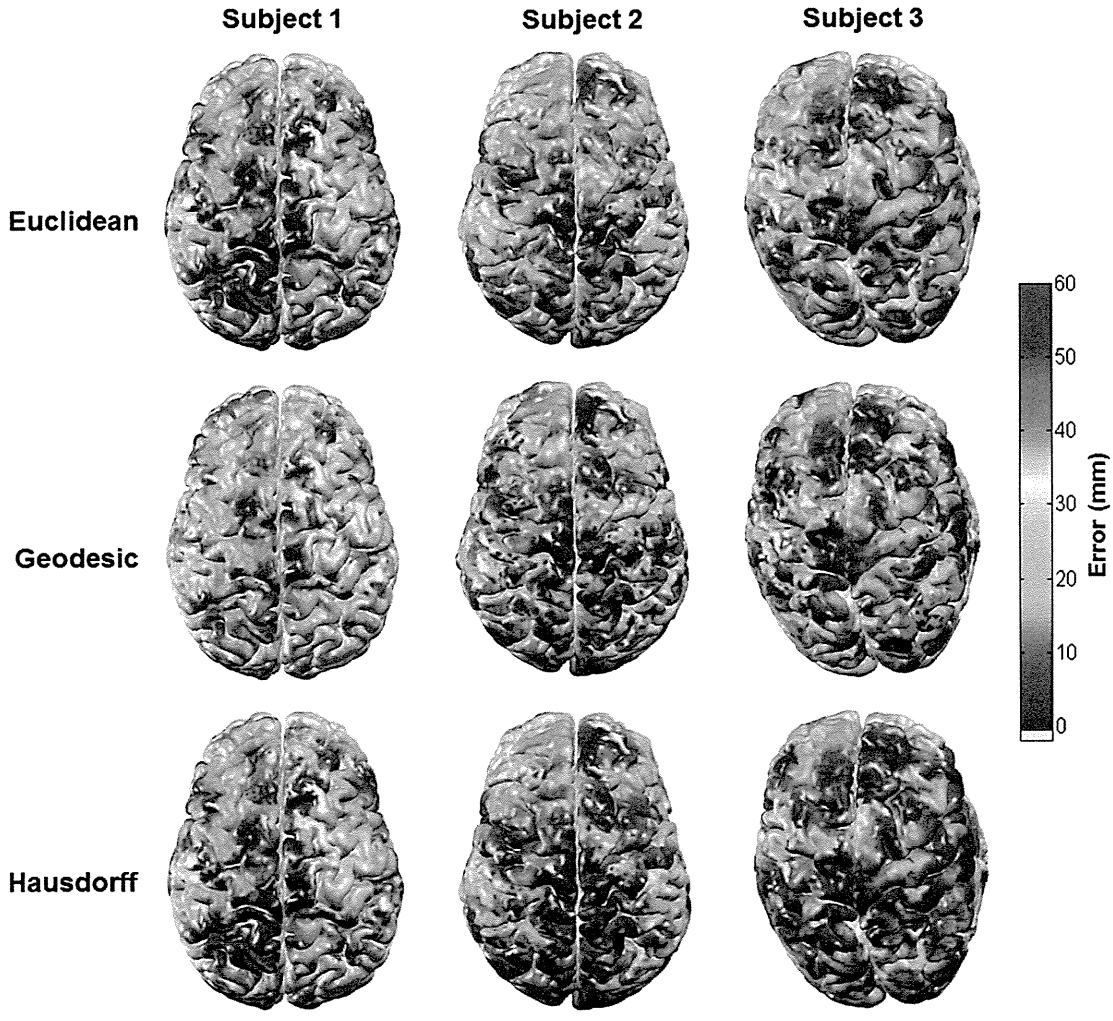

Fig. 7. The three localization error metrics (Euclidean, geodesic and Hausdorff) for atlas-based DOI reconstruction, as a function of cortical position in three subjects. The gray color indicates no assigned value due to a sparsity of simulated activations in those areas.

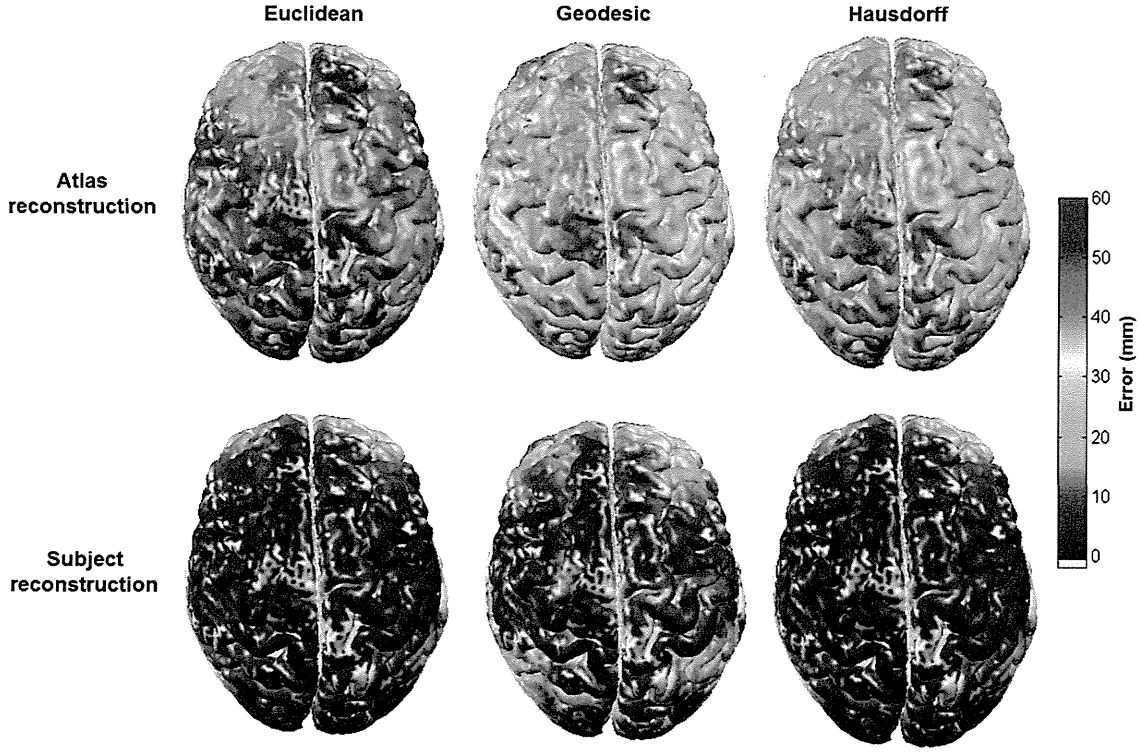

Fig. 8. The mean localization errors across all 32 subjects for atlas-guided and subject MRI-guided DOI as a function of cortical position. The gray color indicates no assigned value due to a sparsity of simulated activations in those areas.

metric, calculated by averaging across the cortex and across all 32 subjects for atlas and subject-MRI processing are given in Table 1.

Discussion

With the application of DOT techniques becoming more common, across a variety of fields, there is a growing need to develop a method which extracts as much of the spatial information present in DOT as possible, while maintaining the advantages the technique has over other neuroimaging modalities; namely convenience, cost and portability. The atlas-guided DOT approach described here and by Custo et al. (2010) meets this requirement. As a prerequisite for its extended application we have investigated and quantified the localization error inherent to atlas-guided DOT.

The localization error of atlas-guided DOT has three fundamental sources. The first is the error in registration of the atlas to the subject surface. This error varies from subject to subject and will depend on the accuracy of the measurement of the cranial landmarks and has been estimated by Singh et al. (2005), to be between 4 and 7 mm. The second is anatomical differences between the subject and the atlas. Even if the affine transformation of the cranial landmarks from the atlas to the subject space is perfectly accurate, there will still be significant differences between the position and folding of the atlas cortex and that of the subject's cortex. Therefore, the contribution of registration and anatomical differences to the cortical localization is likely to be significantly greater than 4–7 mm, particularly in regions of dense cortical folding.

The third factor contributing to the error of atlas-guided DOT is the inaccuracy of diffuse optical image reconstruction itself, which is dependent on the probe geometry and the sensitivity of that probe in a given subject.

The sensitivity of the simulated probe varies across the cortex and across subjects. Regions which have consistently low sensitivity compared to the subject maximum (such as the pre-frontal cortex, Fig. 2) clearly yield high localization errors across subjects, (Figs. 7 and 8). A comparison of Figs. 2 and 7 shows that there are also areas of high localization error in each subject which are not consistent with low probe sensitivity, suggesting that errors in registration and anatomical differences are a significant, if not dominant, source of error in those regions.

The results of our simulation in 32 subject and 32 registered atlas volumes show that the Euclidean error in the localization of brain activations increases two-fold, from 9.1 to 18.0 mm, when an atlas is used in place of the subject's own MRI. The subject-guided localization error of 9.1 mm should be thought of as the error inherent to diffuse optical image reconstruction in regions of the cortex to which our probe is reasonably sensitive. This figure is in good agreement with previous studies. Boas and Dale (2005) found the localization error to be between 5 and 10 mm when using a subject's true anatomy and a similarly dense DOT probe. We can therefore conclude that the additional Euclidean localization error introduced by an atlas-driven approach is on the order of 1 cm.

The significant difference between the Euclidean and geodesic error metrics shown in Fig. 8 suggests that in many cases the centroid of brain activation is incorrectly reconstructed on a neighboring gyrus. The largest geodesic errors occur over the frontal poles and around the posterior temporal lobe (Figs. 7 and 8), which (due to the limits of the virtual probe) are regions of low sensitivity. Although the geodesic error is smaller in regions of good sensitivity (for

Table 1
Grand average localization errors. The average localization errors associated with atlas-guided and subject-MRI guided DOT across all 32 subjects and their standard deviations.

	Mean Euclidean error (mm)	Mean geodesic error (mm)	Mean Hausdorff error (mm)
Atlas-guided DOT	18.0 ± 5.7	30.4 ± 11.4	23.2 ± 5.9
Subject-MRI-guided DOT	9.1 ± 6.7	14.2 ± 13.2	11.1 ± 8.6

example, around the pre-central gyrus, Fig. 8) it still greatly exceeds the Euclidean error. Our results therefore indicate that those applying atlas-based DOT must be extremely cautious in assigning a region of activation to a particular cortical gyrus, particularly in regions of high dense cortical folding. It is important to note that the geodesic error also significantly exceeds the Euclidean error for subject-specific DOT reconstruction in regions of low sensitivity, though the effect is clearly exacerbated by the errors associated with atlas registration and anatomical variation. It is therefore likely that employing a higher density DOT probe would allow greater confidence in localizing activations to specific gyri for both subject-specific and atlas-based DOT (Dehghani et al., 2009).

The Hausdorff distance is a useful metric for quantifying the difference between the shape and size of the reconstructed activations. The fact that the Hausdorff and Euclidean errors are of similar magnitude suggests that the Hausdorff error is generally the result of the shift in position of the peak of activation and that the spatial extent of a simulated activation is, on average, well maintained by DOT.

Fig. 8 shows the localization error metrics averaged across all 32 subjects. It is clear from these figures that there is a consistent spatial pattern of localization error, despite there being significant inter-subject variability (Fig. 7). While it is difficult to comment on its significance, this pattern must arise because of a consistent, spatially varying bias. The source of this error could potentially be consistent anatomical differences between the subjects and the atlas. This is a possibility because the Colin27 atlas (which was chosen because of its high resolution) was produced from the repeated MRI scans of a single subject. However, it is also probable that this bias is a manifestation of the cortically varying sensitivity of the virtual DOT probe, which was applied to every subject.

In conclusion, we have performed a validation of a specific anatomical atlas-guided approach to the analysis of DOT data. Although care should be taken in assigning a hemodynamic response to a particular gyrus, atlas-guided DOT can produce reasonably accurate images of cortical activation, and constitutes a suitable functional imaging approach when a spatial resolution of approximately 2 cm is permitted.

Acknowledgments

This work was supported by NIH P41-RR14075, P41-RR13218, and R01-EB006385 (to D.A.B.), NIH P41-RR-013218 and P41-EB-015902 (to W.W.), Comprehensive Research on Disability, Health and Welfare from Health and Labour Sciences Research Grants (to I.D.), and the Grants-in-Aid for Scientific Research from the Japan Society for Promotion of Science (23390354, and 23650217 to I.D.).

References

Arridge, S.R., 1999. Optical tomography in medical imaging. Inverse Probl. 15, R41–R93.
Austin, T., Gibson, A.P., Branco, G., Yusof, R.M., Arridge, S.R., Meek, J.H., Wyatt, J.S., Delpy, D.T., Hebden, J.C., 2006. Three dimensional optical imaging of blood volume and oxygenation in the neonatal brain. Neuroimage 31, 1426–1433.
Barbour, R.L., Graber, H.L., Chang, J., Barbour, S.-L.S., Koo, P.C., Aronson, R., 1995. MRI-guided optical tomography: prospects and computation for a new imaging method. IEEE Comput. Sci. Eng. 2, 63–77.
Bluestone, A., Abdoulaev, G., Schmitz, C., Barbour, R., Hielscher, A., 2001. Three-dimensional optical tomography of hemodynamics in the human head. Opt. Express 9, 272–286.
Boas, D.A., Dale, A.M., 2005. Simulation study of magnetic resonance imaging-guided cortically constrained diffuse optical tomography of human brain function. Appl. Opt. 44, 1957–1968.
Boas, D.A., Chen, K., Grebert, D., Franceschini, M.A., 2004. Improving the diffuse optical imaging spatial resolution of the cerebral hemodynamic response to brain activation in humans. Opt. Lett. 29, 1506–1508.
Collins, D.L., Zijdenbos, A.P., Kollokian, V., Sled, J.G., Kabani, N.J., Holmes, C.J., Evans, A.C., 1998. Design and construction of a realistic digital brain phantom. IEEE Trans. Med. Imaging 17, 463–468.
Culver, J.P., Choe, R., Holboke, M.J., Zubkov, L., Durduran, T., Slemp, A., Ntziachristos, V., Chance, B., Yodh, A.G., 2003. Three-dimensional diffuse optical tomography in the parallel plane transmission geometry: evaluation of a hybrid frequency domain/continuous wave clinical system for breast imaging. Med. Phys. 30, 235–247.
Custo, A., Boas, D.A., Tsuzuki, D., Dan, I., Mesquita, R., Fischl, B., Grimson, W.E.L., Wells III, W., 2010. Anatomical atlas-guided diffuse optical tomography of brain activation. Neuroimage 49, 561–567.
Dale, A.M., Sereno, M.I., 1993. Improved localization of cortical activity by combining EEG and MEG with MRI cortical surface reconstruction: a linear approach. J. Cogn. Neurosci. 5, 162–176.
Dale, A.M., Fischl, B., Sereno, M.I., 1999. Cortical surface-based analysis: I. Segmentation and surface reconstruction. Neuroimage 9, 179–194.
Dehghani, H., White, B.R., Zeff, B.W., Tizzard, A., Culver, J.P., 2009. Depth sensitivity and image reconstruction analysis of dense imaging arrays for mapping brain function with diffuse optical tomography. Appl. Opt. 48, D137–D143.
Durduran, T., Choe, R., Baker, W.B., Yodh, A.G., 2010. Diffuse optics for tissue monitoring and tomography. Rep. Prog. Phys. 73, 076701.
Fang, Q., 2010. Mesh-based Monte Carlo method using fast ray-tracing in Plücker coordinates. Biomed. Opt. Express 1, 165–175.
Fischl, B., Sereno, M.I., Dale, A.M., 1999. Cortical surface-based analysis: II: inflation, flattening, and a surface-based coordinate system. Neuroimage 9, 195–207.
Fischl, B., Salat, D.H., van der Kouwe, A.J.W., Makris, N., Ségonne, F., Quinn, B.T., Dale, A.M., 2004. Sequence-independent segmentation of magnetic resonance images. Neuroimage 23 (Supplement 1), S69–S84.
Gagnon, L., Perdue, K., Greve, D.N., Goldenholz, D., Kaskhedikar, G., Boas, D.A., 2011. Improved recovery of the hemodynamic response in diffuse optical imaging using short optode separations and state-space modeling. Neuroimage 56, 1362–1371.
Gibson, A.P., Hebden, J.C., Arridge, S.R., 2005. Recent advances in diffuse optical imaging. Phys. Med. Biol. 50, R1–R43.
Gibson, A.P., Austin, T., Everdell, N.L., Schweiger, M., Arridge, S.R., Meek, J.H., Wyatt, J.S., Delpy, D.T., Hebden, J.C., 2006. Three-dimensional whole-head optical tomography of passive motor evoked responses in the neonate. Neuroimage 30, 521–528.
Gregg, N.M., White, B.R., Zeff, B.W., Berger, A.J., Culver, J.P., 2010. Brain specificity of diffuse optical imaging: improvements from superficial signal regression and tomography. Front. Neuroenergetics 2, 1662–6427.
Huppertz, H.-J., Otte, M., Grimm, C., Kristeva-Feige, R., Mergner, T., Lücking, C., 1998. Estimation of the accuracy of a surface matching technique for registration of EEG and MRI data. Electroencephalogr. Clin. Neurophysiol. 106, 409–415.
Huttenlocher, D.P., Klanderman, G.A., Rucklidge, W.A., 1993. Comparing images using the Hausdorff distance. IEEE Trans. Pattern Anal. Mach. Intell. 15, 850–863.
Jöbsis, F.F., 1977. Noninvasive, infrared monitoring of cerebral and myocardial oxygen sufficiency and circulatory parameters. Science 198, 1264–1267.
Jurcak, V., Tsuzuki, D., Dan, I., 2007. 10/20, 10/10, and 10/5 systems revisited: their validity as relative head-surface-based positioning systems. Neuroimage 34, 1600–1611.
Lloyd-Fox, S., Blasi, A., Elwell, C.E., 2010. Illuminating the developing brain: the past, present and future of functional near infrared spectroscopy. Neurosci. Biobehav. Rev. 34, 269–284.
Ntziachristos, V., Yodh, A.G., Schnall, M.D., Chance, B., 2002. MRI-guided diffuse optical spectroscopy of malignant and benign breast lesions. Neoplasia 4, 347–354.
Singh, A.K., Okamoto, M., Dan, H., Jurcak, V., Dan, I., 2005. Spatial registration of multichannel multi-subject fNIRS data to MNI space without MRI. Neuroimage 27, 842–851.
Tsuzuki, D., Jurcak, V., Singh, A.K., Okamoto, M., Watanabe, E., Dan, I., 2007. Virtual spatial registration of stand-alone fNIRS data to MNI space. Neuroimage 34, 1506–1518.
White, B.R., Snyder, A.Z., Cohen, A.L., Petersen, S.E., Raichle, M.E., Schlaggar, B.L., Culver, J.P., 2009. Resting-state functional connectivity in the human brain revealed with diffuse optical tomography. Neuroimage 47, 148–156.
Zeff, B.W., White, B.R., Dehghani, H., Schlaggar, B.L., Culver, J.P., 2007. Retinotopic mapping of adult human visual cortex with high-density diffuse optical tomography. Proc. Natl. Acad. Sci. 104, 12169–12174.

NeuroImage: Clinical 1 (2012) 131–140

Contents lists available at SciVerse ScienceDirect

NeuroImage: Clinical

journal homepage: www.elsevier.com/locate/ynicl

Right prefrontal activation as a neuro-functional biomarker for monitoring acute effects of methylphenidate in ADHD children: An fNIRS study☆

Yukifumi Monden [a,b,1], Haruka Dan [c,1], Masako Nagashima [a], Ippeita Dan [d,*], Daisuke Tsuzuki [d], Yasushi Kyutoku [d], Yuji Gunji [b], Takanori Yamagata [a], Eiju Watanabe [c], Mariko Y. Momoi [a]

[a] Department of Pediatrics, Jichi Medical University, 3311-1 Yakushiji, Shimotsuke, Tochigi 329-0498, Japan
[b] Department of Pediatrics, International University of Health and Welfare, 537-3 Iguchi, Shiobara, Tochigi 329-2763, Japan
[c] Department of Neurosurgery, Jichi Medical University, 3311-1 Yakushiji, Shimotsuke, Tochigi 329-0498, Japan
[d] Functional Brain Science Laboratory, Jichi Medical University, 3311-1 Yakushiji, Shimotsuke, Tochigi 329-0498, Japan

ARTICLE INFO

Article history:
Received 19 June 2012
Received in revised form 1 October 2012
Accepted 3 October 2012
Available online 20 September 2012

Keywords:
Cortical hemodynamics
Developmental disorder
Dorsolateral prefrontal cortex
Optical topography
Ventrolateral prefrontal cortex

ABSTRACT

An objective biomarker is a compelling need for the early diagnosis of attention deficit hyperactivity disorder (ADHD), as well as for the monitoring of pharmacological treatment effectiveness. The advent of fNIRS, which is relatively robust to the body movements of ADHD children, raised the possibility of introducing functional neuroimaging diagnosis in younger ADHD children. Using fNIRS, we monitored the oxy-hemoglobin signal changes of 16 ADHD children (6 to 13 years old) performing a go/no-go task before and 1.5 h after MPH or placebo administration, in a randomized, double-blind, placebo-controlled, crossover design. 16 age- and gender-matched normal controls without MPH administration were also monitored. Relative to control subjects, unmedicated ADHD children exhibited reduced activation in the right inferior frontal gyrus (IFG) and middle frontal gyrus (MFG) during go/no-go tasks. The reduced right IFG/MFG activation was acutely normalized after MPH administration, but not after placebo administration. The MPH-induced right IFG/MFG activation was significantly larger than the placebo-induced activation. Post-scan exclusion rate was 0% among 16 right-handed ADHD children with IQ>70. We revealed that the right IFG/MFG activation could serve as a neuro-functional biomarker for monitoring the acute effects of methylphenidate in ADHD children. fNIRS-based examinations were applicable to ADHD children as young as 6 years old, and thus would contribute to early clinical diagnosis and treatment of ADHD children.

1. Introduction

Attention deficit hyperactivity disorder (ADHD) is characterized by a behavioral phenotype of inattention, hyperactivity and impulsivity, affecting between 3 and 7% of school-aged children in the U.S. (Dittmann et al., 2009; Pietrzak et al., 2006). The symptoms of ADHD can usually be identified during their early elementary school years (Drechsler et al., 2005). Diagnosis of ADHD typically refers to the degree of the symptoms listed in the diagnostic criteria from the DSM-IV (American Psychiatric Association, 1994), which requires rating by the parents or teachers of the children, and thus often entails subjective evaluation. Thus, more objective approaches, preferably based on biomarkers, are a compelling need (Wehmeier et al., 2011; Zhu et al., 2008).

One promising approach is noninvasive functional neuroimaging in combination with neuropsychological tests. A wealth of functional neuroimaging research has started to explore the neural substrates of ADHD. The majority of such research performed thus far has used functional magnetic resonance imaging (fMRI), and many studies have reported less prefrontal activation with ADHD during performance of various cognitive tasks (e.g., Booth et al., 2005; Rubia et al., 1999, 2005; Smith et al., 2006). However, most of the fMRI studies are on adult ADHD patients with only limited implications for children. Among approximately one hundred ADHD-related fMRI studies, twenty-six included patients at the age of eight, eleven at the age of seven (Anderson et al., 2002; Bedard et al., 2010; Booth et al., 2005; Chabernaud et al., 2012; Durston et al., 2007; Fair et al., 2010; Peterson et al., 2009; Slifer et al., 2002; Solanto et al., 2009; Teicher et al., 2000; Vaidya et al., 2005) and only two at the age of six (Durston et al., 2003; Teicher et al., 2000).

The scarcity of child ADHD studies is due to technical obstacles. Severely hyperactive children could not be included in the studies because motion artifacts would have prevented successful

* Corresponding author. Tel.: +81 285 58 7590; fax: +81 285 44 5147.
E-mail address: dan@jichi.ac.jp (I. Dan).

[1] These two authors contributed equally to this work.

2213-1582/$ – see front matter © 2012 The Authors. Published by Elsevier Inc. All rights reserved.
http://dx.doi.org/10.1016/j.nicl.2012.10.001

fMRI measurement (Vaidya et al., 1998). This leads to a high elimination rate due to excessive motion artifacts: One study enrolling a relatively young childhood sample (6 years and older) rejected 50% of ADHD subjects and 30% of normal control subjects (Durston et al., 2003). This further leads to a skewed distribution of the sample: Since motion problems are generally more severe for patients with hyperactivity, the resulting subject pool might be enriched with mildly and predominantly inattentive type patients (Epstein et al., 2007). Moreover, ADHD children may be withdrawn for various reasons related to their symptoms including refusal to enter the MRI scanner, refusal to begin or finish a run after entering the MRI scanner, inattention such as forgetting task rules, and falling asleep (Yerys et al., 2009).

Alternatively, functional near-infrared spectroscopy (fNIRS) is relatively immune to these problems, and has been successfully adopted in tasks involving body movement (Herrmann et al., 2004, 2005; Hock et al., 1997; Matsuo et al., 2000; Moriai-Izawa et al., 2012; Okamoto et al., 2004b; Shinba et al., 2004; Suto et al., 2004). Moreover, fNIRS offers other advantages including its compact size (useful in confined experimental settings), affordable price, unrestrictiveness and accessibility, serving as a suitable choice for clinically assessing ADHD children. A growing body of fNIRS studies has started to investigate the cortical hemodynamics of ADHD patients (Ehlis et al., 2008; Inoue et al., 2012; Negoro et al., 2010; Schecklmann et al., 2008, 2010; Weber et al., 2005). Most typically, a recent study focusing on Stroop interference revealed that the right prefrontal cortex oxy-Hb increase due to Stroop interference was reduced in ADHD children, suggesting a dysfunction of the area (Jourdan Moser et al., 2009).

The advent of fNIRS raised the possibility of introducing neuroimaging diagnosis in younger ADHD children, and this might further lead to its application in early clinical treatment. The most common treatment for ADHD children is the administration of methylphenidate (MPH), a psychostimulant drug that has been shown to be effective in improving attention and behavior as well as cognition and social function (Spencer, 2004). The behavioral and cognitive characteristics of ADHD are considered to be partly due to dopamine and noradrenaline dysfunction (Wilens, 2008). MPH is considered to inhibit reuptake of catecholamines, including dopamine, by blocking their transporters and to act as a dopamine agonist in the basal ganglia and cerebral cortices (Arnsten, 2006). A recent longitudinal study reported that the use of MPH to treat children and adolescents with ADHD may be conducive to enhancing educational outcomes by reducing the likelihood of disruptive behavior (Biederman et al., 2009). To confer long-term positive effects of treatment and thereby increase the quality of life of ADHD children, early identification of ADHD and appropriate treatment are important. This led us to postulate that fNIRS would be effective in monitoring the effect of MPH in ADHD children, especially for younger children who are difficult to assess in an fMRI environment.

Response inhibition as measured by go/no-go tasks has emerged as one of the principal paradigms for studying ADHD (Aron and Poldrack, 2005). Using this task, it has been clearly demonstrated that children (Beauregard and Levesque, 2006; Derefinko et al., 2008; Durston et al., 2003; Inoue et al., 2012; Ma et al., 2012; Monden et al., 2012; Siniatchkin et al., 2012; Smith et al., 2006; Solanto et al., 2009; Vaidya et al., 1998), adolescents (Schulz et al., 2004; Tamm et al., 2004) and adults (Dibbets et al., 2009; Karch et al., 2010; Mulligan et al., 2011; Sebastian et al., 2012; Vasic et al., in press) with ADHD have response inhibition deficits. An extensive review of functional neuroimaging in healthy adults indicates that widespread regions of the frontal cortex, especially the right inferior frontal gyrus (IFG), are associated with response inhibition (Aron and Poldrack, 2005). Structural neuroimaging in ADHD has fairly consistently indicated gray matter density reductions in the striatum and right IFG (Durston et al., 2004). A former fMRI study on ADHD children with an MPH history reported that MPH increased the activation of the frontal cortices and striatum in go/no-go tasks (Vaidya et al., 1998). The specificity of the implicated brain regions in healthy subjects, as well as functional and structural changes to those regions in ADHD patients, suggests that response inhibition is a good neuro-functional biomarker candidate for ADHD (Aron and Poldrack, 2005).

Thus, using the decrease of IFG activation during a response inhibition task as a potential neuro-functional biomarker for ADHD, we aimed to establish a robust procedure for detecting its recovery with MPH administration. Our initial effort (Monden et al., 2012) was to test whether fNIRS-based diagnosis could be introduced in actual clinical situations. We demonstrated that fNIRS could monitor the cortical hemodynamics of ADHD children (7 to 14 years old) performing a go/no-go task before and 1.5 h after MPH administration, allowing the observation of the acute effect of MPH as a significant increase in the oxy-Hb signal in the right lateral prefrontal cortex. As the monitoring takes only a few minutes, we further showed that the entire process can be implemented within a single-day hospital visit.

However, since that study was optimized for assessing the feasibility of introducing fNIRS as an actual clinical tool that allows the pre- and post-medication comparison to be performed in a single-day hospital visit, a neuro-pharmacological examination of the effects of MPH on ADHD children has yet to be performed. Thus, in the current study, enrolling sixteen ADHD children and age/sex-matched healthy control children, we examined the pharmacological effects of MPH on the cortical hemodynamics of ADHD during a go/no-go task. Subjects received either MPH or a placebo in a randomized, double-blind, placebo-controlled, crossover design. We hypothesized that MPH would modulate hemodynamic responses in the right prefrontal cortex during a go/no-go task while a placebo would not, and assessed this hypothesis using fNIRS. Moreover, we desire to validate the feasibility of introducing fNIRS-based diagnosis of the effects of MPH administration to ADHD children of 6 years old, the earliest age at which the FDA recommends starting MPH administration.

2. Material and methods

2.1. Subjects

Sixteen clinically referred, right-handed Japanese children with a mean age of 8.8 (SD 2.2, range 6–13 years) who met the DSM-IV criteria for ADHD participated in the study (Table 1). The subject group differed from the previous study (Monden et al., 2012). The Wechsler Intelligence Scale of Children—Third Edition (WISC-III) full IQ scores of subjects were all over 70 (mean 90.3, SD 10.0, range 74–110). Sixteen right-handed control subjects were matched with the ADHD subjects according to age (mean 8.9, SD 2.4, range 6–13 years) and gender (10 boys and 6 girls). IQs of controls (mean 111.8, SD 8.7, range 99–135) were significantly ($t=6.40$, $p<0.0001$) higher than those of ADHD subjects. Written consent was obtained from the parents of all subjects. The study was approved by the Ethics Committees of Jichi Medical University Hospital, and the International University of Health and Welfare. The study was in accordance with the latest version of the Declaration of Helsinki. This study was registered to UMIN-CTR Clinical Trial (UMIN000006277) as "Neurophysiological analysis in developmental disorders: an exploratory neuroimaging study using functional near-infrared spectroscopy (fNIRS)".

2.2. Experimental design

The effects of MPH were examined in a randomized, double-blind, placebo-controlled, crossover study while the subjects performed a go/no-go task. Experimental procedure is summarized in Fig. 1. ADHD subjects were examined twice (the times of day for both measurements were scheduled to be as close as possible), at least 4 days apart, but within 30 days. Control subjects only underwent a pre-administration session.

On each examination day, ADHD subjects underwent two sessions, one before drug (MPH or placebo) administration, and the other at 1.5 h after the drug administration. Each session consisted of 6 block

Table 1
Demographic and clinical profiles for ADHD subjects.

ID	Age (years)	Sex	ADHD subtype	Complication	WISC-III full IQ	MPH dose (mg)	Duration of MPH exposure (years)	Other medications
1	7	M	Inattentive	None	110	18	1.0	None
2	8	M	Combined	None	95	27	1.0	None
3	12	M	Combined	PDD	96	27	1.8	None
4	11	M	Combined	None	82	27	3.4	None
5	6	F	Hyperactive	None	98	18	0.6	None
6	7	M	Combined	PDD	79	18	Naïve	None
7	13	M	Combined	None	82	45	2.1	Carbamazepine, risperidone
8	8	F	Combined	PDD	85	18	Naïve	None
9	8	F	Combined	Epilepsy	85	18	Naïve	Valproic acid
10	8	M	Combined	PDD	101	18	2.0	None
11	8	M	Combined	None	90	27	2.2	None
12	7	M	Combined	None	95	18	Naïve	None
13	6	F	Inattentive	None	74	18	Naïve	None
14	10	M	Combined	None	105	18	Naïve	None
15	9	M	Combined	None	85	18	Naïve	None
16	12	M	Combined	None	90	18	0.1	None
Mean	8.8				90.8			
SD	2.2				9.9			

Abbreviations: SD, standard deviation; PDD: pervasive developmental disorders.

sets, each containing alternating go (baseline) and go/no-go (target) blocks. Each block lasted 24 s and was preceded by instructions displayed for 3 s, giving an overall block-set time of 54 s and a total session time of 5.5 min. In the go block, subjects were presented a random sequence of two pictures and asked to press a button for both pictures. In the go/no-go block, subjects were presented with a no-go picture 50% of the time, thus being required to respond to half the trials (go trials) and inhibit their response to the other half (no-go trials). A go/no-go ratio of 50% was selected as it has been most often used in former neuroimaging studies (Dillo et al., 2010; Herrmann et al., 2005; Liddle et al., 2001; Menon et al., 2001; Vaidya et al., 1998). Pictures were presented with 1 Hz frequency during go and go/no-go blocks. At the beginning of each block, instructions (e.g., "press for tiger or elephant" for go conditions and "do not press for giraffe" for go/no-go conditions) were displayed for 3 s to inform the subject about the new block. Each subject performed a practice block before any measurements to ensure their understanding of the instructions.

After ADHD subjects performed the first session, either MPH (OROS-methylphenidate or Concerta) or a placebo was administered orally. Specific acute doses were the same as their daily dose as described in Table 1.

2.3. fNIRS measurements

We used the multichannel fNIRS system ETG-4000 (Hitachi Medical Corporation, Kashiwa, Japan), using two wavelengths of near-infrared light (695 and 830 nm). We analyzed the optical data based on the modified Beer–Lambert Law (Cope et al., 1988) as previously described (Maki et al., 1995).

We set the fNIRS probes to cover the lateral prefrontal cortices in reference to previous studies (Garavan et al., 1999; Herrmann et al., 2004, 2005; Liddle et al., 2001; Monden et al., 2012; Rubia et al., 2003), resulting in 22 channels (CH) per hemisphere. The specific setting was as previously described (Monden et al., 2012). After the fNIRS measurement, positional data of illuminators and detectors were obtained for both the ADHD and control subjects using a 3D-digitizer (Fastscan, Polhemus), and subjected to probabilistic registration of fNIRS channel positions to MNI space (Jurcak et al., 2007; Okamoto et al., 2004a; Okamoto and Dan, 2005; Singh et al., 2005; Tsuzuki et al., 2007, 2012) with reference to macroanatomical brain atlases (Rorden and Brett, 2000; Shattuck et al., 2008).

Oxy-Hb signals were used for further analysis due to its higher signal amplitude than that of deoxy-Hb (Strangman et al., 2002). Individual timeline data for the oxy-Hb signals of each channel were preprocessed with a first-degree polynomial fitting and high-pass filter using cut-off frequencies of 0.01 Hz to remove baseline drift, and a 0.8 Hz low-pass filter to remove heartbeat pulsations. After removal of blocks with marked motion-related artifacts, timeline data of the remaining blocks (where more than 4 blocks remained) were used. From the preprocessed time series data, we obtained channel-wise and subject-wise contrasts by calculating the inter-block means of difference between the target (4–24 s after go/no-go block onset) and baseline (14–24 s after go block onset) periods.

2.4. Statistical analyses

We performed statistical analyses in a channel-wise manner on oxy-Hb signals. Specifically, for control subjects who were examined only once, the target vs. baseline contrast of the session was generated. For ADHD subjects, the following contrasts were generated: (1) first-day, pre-medication contrast: target vs. baseline contrast for the pre-medication condition (either placebo or MPH administration) for the first day exclusively; (2) pre-medication contrasts: target vs. baseline contrast for the pre-placebo and pre-MPH conditions (for either first or second day measurements); (3) post-medication contrasts (specifically, post-placebo and post-MPH contrasts): target vs. baseline contrast for the post-placebo and post-MPH conditions; (4) intra-medication contrasts: difference between post- and pre-medication contrast for each medication (i.e., intra-placebo and intra-MPH contrasts); and (5) inter-medication contrast: difference between intra-MPH and intra-placebo contrasts. Note that (2) and (4) were generated temporally for calculating (5).

To screen the channels involved in go/no-go tasks in normal control subjects, target vs. baseline contrasts were subjected to one-sample *t*-tests against zero (two-tails). Statistical threshold was set at 0.05 with Bonferroni method for family-wise error correction. For thus-screened channels, comparisons between control and ADHD were performed for the following three ADHD contrasts: (1) first-day, pre-medication, (2) post-placebo, and (3) post-MPH. They were subjected to independent two-sample *t*-tests (two-tails) with a statistical threshold of $p<0.05$. For examining medication effects on ADHD subjects, comparison between intra-MPH and intra-placebo (i.e., inter-medication contrast) was subjected to one-sample *t*-tests against zero (two-tails) with a statistical threshold of $p<0.05$.

2.5. Behavioral data analysis

The reaction time (RT) of go trials, and accuracy (ACC) for go and no-go trials were computed for each go/no-go block. ACCs and RTs were averaged across go/no-go blocks, and subjected to statistical

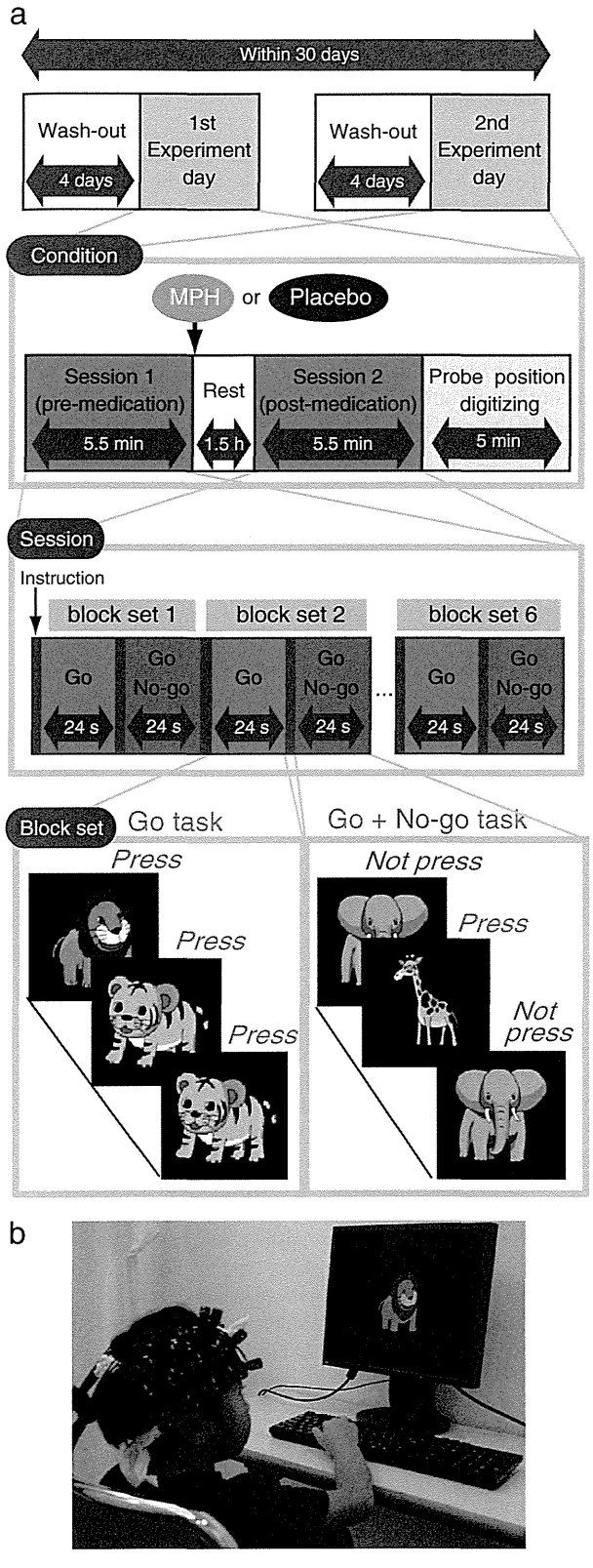

Fig. 1. Experimental design. a. A schematic showing the flow of pre- and post-medication administration sessions for ADHD subjects. b. fNIRS measurements. Brain activity was measured while ADHD and control subjects performed the go/no-go task.

analyses as described in the previous section. Statistical threshold was set at 0.05 with Bonferroni method for multiple-comparison error correction (i.e., significant p was $<0.05/3$).

3. Results

3.1. Behavioral performance

The average ACC for go and no-go trials and RT for correct go trials in the go/no-go block for control and ADHD subjects are summarized in Table 2. In ADHD subjects, the first-day data before administration of either a placebo or MPH was used as a representation of pre-medication contrast. Second-day data was excluded for this contrast.

First-day pre-medication, post-placebo, and post-MPH values of ADHD subjects were compared with values for control subjects (Table 2). Significant differences in ACC for no-go trials were found between control subjects and first-day pre-medication ADHD subjects and between control subjects and post-placebo ADHD subjects.

For analysis within each ADHD subject, the inter medication contrast comparing the effect of MPH against the placebo revealed no significant differences in behavioral parameters (Table 3).

3.2. fNIRS analyses

We screened for any fNIRS channels involved in the go/no-go task for the control subjects. Significant oxyHb increase was found in the right CH 10 (mean 0.075, SD 0.074, $p<0.05$, Bonferroni-corrected, Cohen's $d = 1.009$). This channel was located in the border region between the right MFG and IFG (MNI coordinates x,y,z (SD): 46,43,30 (14), MFG 78%, IFG 22% with reference to macroanatomical brain atlases (Rorden and Brett, 2000; Shattuck et al., 2008)). Thus, we set the right CH 10 as a region-of-interest (ROI) for the rest of the study. For reference, cortical activation patterns with all the channels are presented for control and ADHD subjects as supplementary material.

Comparison between oxy-Hb signals of the control and first-day pre-medicated ADHD subjects revealed significantly higher oxy-Hb signal in the right CH 10 in the control subjects (independent two-sample t-test, $p<0.05$, Cohen's $d = 0.839$, Table 2). This indicates that the control subjects exhibited higher right prefrontal activation during go/no-go tasks than did the pre-medicated ADHD children.

Effects of medications were examined between control and post-placebo ADHD subjects, and between control and post-MPH ADHD subjects (independent two-sample t-test, thresholded at $p<0.05$). Oxy-Hb signal in control was significantly higher than in post-placebo ADHD subjects, whereas no significant difference was found for those in control and post-MPH ADHD subjects (Table 2). This suggests that the impaired right prefrontal activation in pre-medicated ADHD subjects was normalized by the MPH administration.

Finally, we tested whether there was an MPH-induced, but not placebo-induced, right prefrontal activation in ADHD children. In the inter-medication contrast, the right CH 10 was found to be significant with a large effect size (one-sample t-test, $p<0.05$, Cohen's $d = 0.952$, Table 3). This result indicates that the oxy-Hb signal increase during go/no-go tasks was induced by MPH but not by the placebo.

3.3. Oxy-Hb timeline data

Fig. 2 illustrates the grand average waveforms of all 16 control subjects and 16 ADHD subjects. For ADHD, oxy-Hb and deoxy-Hb signals are presented for pre-/post-placebo and pre-/post-MPH conditions on CH 10 of the right hemisphere. We observed more stable task-related oxy-Hb signals than deoxy-Hb signals, suggesting the robustness of oxy-Hb signals for our experimental conditions. An oxy-Hb increase in the right CH 10 was clearly observed for control and post-MPH administration of ADHD in the grand average waveform. Waveforms for individual subjects (subject 5: 6-year-old ADHD girl, and subject 1: 7-year-old ADHD boy) are also illustrated. Although the individual data resulted in somewhat noisy waveforms,

Table 2
Go/no-go task performance and functional data for control and ADHD subjects.

	Control		ADHD									
			1st day pre-medication				Post-placebo			Post-MPH		
	Mean	SD	Mean	SD	t	p	Mean	SD	t	p	Mean	SD	t	p
ACC for go trials (%)	96.5	5.48	86.2	21.9	1.829	0.085^{ns}	85.3	20.2	2.14	0.047^{ns}	92.3	12.0	1.266	0.219^{ns}
ACC for no-go trials (%)	95.2	4.52	86.6	11.9	2.688	0.014^{*}	86.5	8.46	3.634	0.001^{**}	89.5	8.51	2.347	0.028^{ns}
RT for correct go trials (ms)	421.4	57.5	385.5	96.8	1.275	0.214^{ns}	377.0	83.6	1.753	0.091^{ns}	404.9	47.9	0.881	0.386^{ns}
Oxy-Hb right CH10 (mM·mm)	0.075	0.074	0.008	0.084	2.374	0.024^{*}	0.001	0.087	2.586	0.015^{*}	0.077	0.060	−0.110	0.916^{ns}

Performance data (ACC and RT) is presented for go and no-go trial data from go/no-go blocks. Oxy-Hb values for right CH10 are presented as functional data. For ADHD subjects, data for 1st day pre-medication, post-medication of placebo and MPH are shown. t-value, p-value and statistical significance were the results of t-tests between control and each ADHD condition. Abbreviations: SD, standard deviation; t, t-value; p, p-value. Statistical significances are presented as follows: *, $p<0.05$; **, $p<0.01$; and ns, not significant.

the oxy-Hb activation in the post-MPH session is clearly presented even in the data of the 6-year-old ADHD subject.

3.4. Examination on the effects of IQ

Since we did not match the IQ of the ADHD and normal healthy control subjects, we performed additional analyses to find the possible effects of IQ. We examined the correlation between IQ and activation in the right CH 10 for ADHD children (ADHD 1st day pre-medication contrast) and normal healthy control children, respectively. In ADHD children, Pearson's correlation coefficient was 0.184 ($p=0.494$), while that in control children was 0.010 ($p=0.969$): Neither analysis yielded any significant correlation with a meaningful effect size. In addition, we examined whether the two correlation coefficients were different, but did not find any significant difference (Fischer's $z=0.45$, $p>0.05$). Thus we concluded there was no correlation between IQ and the activation in the right CH 10 in either group.

4. Discussion

The current study exploring fNIRS-based diagnosis of the effects of MPH administered to ADHD children revealed that the right IFG/MFG activation could serve as an objective neuro-functional biomarker for fNIRS measurement. First, relative to control subjects, unmedicated ADHD children exhibited reduced brain activation in the right IFG/MFG during go/no-go task blocks. Second, the reduced right IFG/MFG activation was acutely normalized after MPH administration, but not after placebo administration. Third, the MPH-induced right IFG/MFG activation was significantly larger than the placebo-induced activation.

4.1. Behavioral performance for go/no-go task

The current fNIRS analyses adopted the contrast of go/no-go against go tasks. In addition to response inhibition, this contrast is thought to commeasure additional cognitive functions, including decision making, response competition/response selection, conflict monitoring, and increased attentional demand (Liddle et al., 2001; Menon et al., 2001; Rubia et al., 2001, 2003). Thus, the fNIRS results are expected to reflect a rather wide spectrum of cognitive functions associated with ADHD. On the other hand, neuropsychological tests are expected to examine specific cognitive aspects of ADHD symptoms. Go errors (omission errors) are typically considered indicators of inattention to the task, while no-go errors (commission errors) and RT to go responses are considered indicators of impulsivity (Barkley, 1991; Newcorn et al., 2001). Numerous studies have demonstrated that MPH improves no-go indices in child and adult ADHD patients (Aron et al., 2003; Aron and Poldrack, 2005; Bedard et al., 2003; Tannock et al., 1995). However, MPH also affects the speed of go responses, go response variability, and discrimination errors in go trials (Aron and Poldrack, 2005; Bedard et al., 2003; Tannock et al., 1995). Moreover, Rubia et al. suggested that the beneficial MPH effects were more pronounced for inattention problems (reflected by omission errors) than impulsivity (reflected by commission errors) (Rubia et al., 2009).

In the current study, the comparison between controls and unmedicated ADHD patients showed a significantly higher commission

Table 3
ADHD inter-medication (placebo vs. MPH) comparison.

	Mean	SD	t	p
ACC for go trials (%)	1.98	8.12	0.975	0.345^{ns}
ACC for no-go trials (%)	0.03	11.2	0.011	0.991^{ns}
RT for correct go trials (ms)	0.84	54.3	0.062	0.951^{ns}
Oxy-Hb right CH10 (mM·mm)	0.084	0.088	3.809	0.002^{**}

Abbreviations: SD, standard deviation; t, t-value; p, p-value. Statistical significances are presented as follows: *, $p<0.05$; **, $p<0.01$; and ns, not significant.

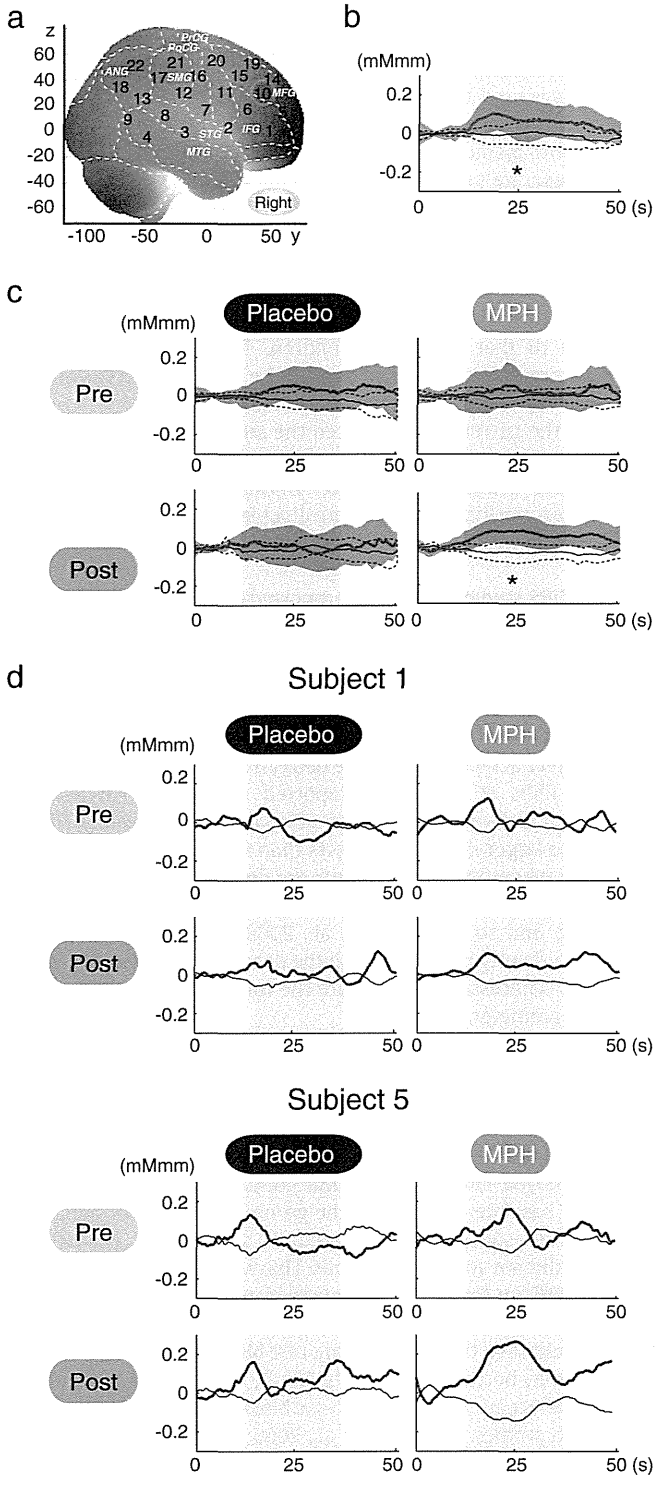

Fig. 2. The channel location and waveforms of oxy-Hb (red line) and deoxy-Hb (blue line) signals for right CH 10. The green area indicates the go/no-go task period. Significant (one-sample *t*-test, $p<.05$) conditions are indicated by asterisks. a. On-brain channel locations (right hemisphere) are statistically estimated for the group of subjects (including both ADHD and control) and exhibited in MNI space. CH 10 is indicated in red. b. Grand averages for control subjects. Standard deviations among the 16 subjects are exhibited as pale red (oxy-Hb) and blue dotted (deoxy-Hb) areas. Each time line is adjusted to the average value for a baseline period of zero. Oxy-Hb and deoxy-Hb signals are shown in units of mM·mm. c. Grand averages for ADHD subjects for pre-/post- and placebo/MPH conditions are illustrated. d. Graphs for ADHD individuals for pre-/post- and placebo/MPH conditions. Subject 1 is a 7-year-old boy and subject 5 is a 6-year-old girl (corresponding to Table 1).

error rate for ADHD subjects. This result was mostly in line with former studies. We detected no significant behavioral performance differences in the MPH-medicated ADHD children contrasted against control subjects, suggesting an MPH effect for no-go performance. However, the inter-condition contrast representing MPH effects against placebo failed to yield any significant behavioral performance change. Although behavioral parameters may often well reflect specific cognitive aspects of ADHD symptoms or MPH effects on them, the current study could not confirm a normalization effect of MPH (but not placebo) on behavioral parameters.

4.2. Right IFG/MFG activation as a robust neuro-functional biomarker

On the other hand, fNIRS may provide more robust measures of MPH effects. Previous neuroimaging studies have elucidated the neural correlates of go/no-go tasks (Simmonds et al., 2008), including the bilateral IFG, MFG and SFG (superior frontal gyrus), supplementary motor area, anterior cingulate gyrus, inferior parietal and temporal lobes, caudate nucleus, and cerebellum (Rubia et al., 2003). The IFG may be specifically related to motor response inhibition, while the MFG/SFG, medial prefrontal, and parietal cortices possibly mediate more general meta-motor executive control functions such as motor attention, conflict monitoring, and response selection, necessary for inhibition task performance (Rubia et al., 2001).

Among these regions, our fNIRS measurements covered the right and left IFG (BA 44/45), MFG (BA 46/9), and SMG (supramarginal gyrus, BA40), and we found activation in the right MFG and IFG (BA9, 46, 45) during the go/no-go task period in the control subjects, but not in the first-day, pre-medicated ADHD subjects. These results suggest that the right prefrontal function associated with the go/no-go task performance was impaired in ADHD children. The administration of a placebo did not result in right prefrontal activation, while that of MPH led the ADHD children to exhibit a degree of right prefrontal activation comparable to that of the normal control subjects. Moreover, the right prefrontal activation due to MPH administration was significantly higher than that due to placebo administration. These results led us to conclude that MPH had significant effects in normalizing right frontal dysfunctions in ADHD children.

The right prefrontal dysfunction and MPH-elicited recovery observed by fNIRS are consistent with former studies using other neuroimaging modalities. A recent ALE meta-analysis of go/no-go tasks (Buchsbaum et al., 2005) reported a mainly right-lateralized network associated with response inhibition, including the right MFG and IFG (BA46/44), the right SMG (BA40), and the superior medial frontal gyrus (BA6) (Simmonds et al., 2008). These regions have been implicated in the processes of stimulus recognition, maintenance and manipulation of stimulus–response associations and response selection, including selecting not to respond (Grafton et al., 1992; Law et al., 1997; Liddle et al., 2001; Mostofsky et al., 2003; Rubia et al., 2001), all of which are critical to the performance of go/no-go tasks (Simmonds et al., 2008). fMRI studies of the go/no-go task have consistently recruited frontal cortices; however, localization and the extent of frontal activation vary across these studies, with activation most often localized to the right IFG (BA 45/47) (Durston et al., 2002; Garavan et al., 1999; Konishi et al., 1999; Rubia et al., 2001), followed by the right MFG/SFG (BA9/46) (Garavan et al., 1999, 2002, 2003, 2006; Hester et al., 2004; Mostofsky and Simmonds, 2008). An fNIRS study also added further evidence to the involvement of the right lateral prefrontal cortex (more exactly, F4) during go/no-go tasks (Boecker et al., 2007). Another recent fNIRS study reported reduced prefrontal activation in ADHD children compared to normal controls during a go/no-go condition (albeit no laterality was reported) (Inoue et al., 2012). Moreover, recent fMRI studies on MPH-medicated children have provided more direct evidence for cortical activation and MPH treatment. Using a continuous performance task, Rubia et al. (2009) found that MPH treatment improved underactivation in ADHD children compared to normal children by adding

activation in the right IFG and MFG along with several other regions (Monden et al., 2012). Therefore, it would be relevant to suggest that normalized right IFG/MFG activation induced by MPH administration during go/no-go task serves as a robust neuro-functional biomarker for fNIRS assessment of MPH effect on ADHD children.

4.3. Effects of IQ

We did not match the IQs of ADHD and normal healthy control children. However, this did not seem to cause any serious effects on the findings of the current study, as we did not find any correlation between IQ and the activation in the right CH 10 in either group. There have been arguments over whether to match IQ or not in ADHD studies. The IQs of ADHD children are lower than those of normal healthy children (Frazier et al., 2004; Kuntsi et al., 2004), and an extensive epidemiological study reported that the co-occurrence of ADHD and low IQ has a genetic overlap (de Zeeuw et al., 2012). Therefore, it is not considered appropriate to treat IQ as a covariant of ANCOVA type of studies (de Zeeuw et al., 2012; Dennis et al., 2009). If IQ had been used as a covariant, the differences in cortical activation in ADHD and normal healthy control children would have been over-corrected since IQ is relevant to the brain phenotype of the disorder (de Zeeuw et al., 2012).

Moreover, IQ measurement of ADHD children poses a problem intrinsic to ADHD symptoms: it is sometimes difficult for young ADHD children to execute IQ tests as they are not always sufficiently patient. Thus, the IQs of ADHD children might be underestimated, and not adequately reliable.

Previous reports adopting an IQ match between ADHD and normal healthy children enrolled ADHD children with relatively high IQs (Aron et al., 2003; Booth et al., 2005; Chabernaud et al., 2012; Durston et al., 2007; Ma et al., 2012; Negoro et al., 2010; Schecklmann et al., 2010; Vaidya et al., 1998; Yerys et al., 2009). Most of these studies excluded low-IQ ADHD children with criteria such as IQ > 85 or IQ > 90 (Aron et al., 2003; Ma et al., 2012; Vaidya et al., 1998; Yerys et al., 2009). We calculated the average IQ of ADHD children in these studies and found that it was 108 ± 8 (mean $\pm$ SD). There is a possibility that low-IQ ADHD children with severe behavioral rating scores had been selectively excluded.

On the other hand, our IQ criterion was greater than 70, which is among the most lenient criterions together with two other recent studies (Inoue et al., 2012; Negoro et al., 2010). Such samples are expected to represent the ADHD population in a balanced manner as they include severe patients. While there might be other possibilities for matching ADHD IQs with those of normal healthy children with low IQs, it is difficult to match the IQs of normal healthy children to those of ADHD groups including children with low IQs, and no study has performed matching for such low scores. Moreover, even if IQ matching had been realized, such samples would not have represented general healthy children.

Although IQ matching for ADHD and control children poses several problems as mentioned above, we do not mean that it should be avoided. Rather, IQ-matching studies should be pursued with different perspectives, such as to assess the effects of IQ, and should be undertaken in the future. As de Zeeuw reported (de Zeeuw et al., 2012), the brains of low-IQ ADHD children might undergo different functional and anatomical development. If this is the case, subdividing the whole group to yield low-IQ groups would be of great clinical importance. For this purpose, the current system, which can measure severely ADHD children with low IQs, would serve as a valuable tool.

4.4. Limitations

A few limitations should be noted for adequate understanding of the current findings. First, a learning effect associated with go/no-go tasks cannot be excluded from the current experimental design: while control subjects underwent only one task session, ADHD children underwent two sessions in the same day. Thus, the effects of habituation (Fischer et al., 2003; Kiehl and Liddle, 2003; Loubinoux et al., 2001) and procedural learning (Eliassen et al., 2001) could be present. First-day pre-medicated data (i.e., either pre-placebo or pre-MPH) was used for the ADHD group to compare the two groups (ADHD and control) under conditions not affected by these factors. However, post-medication data are by necessity from the second sessions. For separate sessions of the same task, an activation of greater magnitude has been observed for the first session for go/no-go tasks in fMRI studies (Langenecker and Nielson, 2003). Thus, it was expected that the oxy-Hb amplitude of the second, post-medicated, sessions would be reduced. However, in the current study, MPH administration to ADHD children still led to increased oxy-Hb amplitude comparable to that of control children. This indicates that MPH exerted pharmacological effects beyond the level needed to compensate for the expected habituation and learning effects.

Second, the current study limited the analyses to the oxy-Hb parameter because we did not find any channels with significant activation with the deoxy-Hb parameter during the screening process performed on normal healthy control subjects. Thus, we concluded that deoxy-Hb was not suitable for further analysis in the current study.

Many fNIRS studies have solely reported the results of the oxy-Hb parameter, including an ADHD study by Negoro et al. (2010). There is a tendency that oxy-Hb is more sensitive than deoxy-Hb (e.g. Ehlis et al., 2008; Inoue et al., 2012; Weber et al., 2005), but the precise reason for the decreased sensitivity of deoxy-Hb has yet to be elucidated. Our previous study adopting a similar experimental paradigm also failed to detect activation with the deoxy-Hb parameter (Monden et al., 2012). Ehlis et al. (2008) reported that deoxy-Hb behavior was different between ADHD and normal subjects: deoxy-Hb decreases were larger in ADHD subjects than in normal subjects. In addition, even when oxy-Hb increased, the deoxy-Hb parameter either increased, remained unchanged or decreased depending on tasks, regions, age and so on (Ehlis et al., 2008; Sakatani et al., 1999), suggesting difficulty in dealing with the deoxy-Hb parameter. Further exploration is necessary to elucidate the role and applicability of the deoxy-Hb parameter.

4.5. Clinical utility of fNIRS-based examination

In the current study, we adopted a go/no-go task paradigm with alternating go and go/no-go blocks. Tsujii et al. (2011) and Cui et al. (2011) employed alternating go and go/no-go tasks, and used the go task as a baseline contrast for the go/no-go task fNIRS signal that they were interested in. Similarly, we used the go block as a baseline period, and did not adopt rest periods. This was primarily because it is extremely difficult for ADHD patients to stay still without performing any task: it may lead to unexpected movements or behaviors. Secondarily, we could save time by omitting rest blocks: a prolonged experiment time may bore ADHD subjects. Finally, experimental paradigms employing alternate go and go/no-go blocks have been commonly used in fMRI studies (Altshuler et al., 2005; Dillo et al., 2010; Ma et al., 2012; Vaidya et al., 1998) and also in fNIRS studies (Tsujii et al., 2011). Thus, considering comparisons across modalities, the choice of experimental paradigm in the current study is appropriate.

An additional merit of the alternative task paradigm is that go blocks can serve as a motor control for go/no-go blocks. Schecklmann et al. (2008) performed weekday reciting task and word fluency tasks and used the weekday reciting task as a baseline to which fNIRS signal during the word fluency tasks was compared. By using a control condition with a similar motor output, movement and muscle artifacts in a task condition are expected to be cancelled. Similarly, we adopted the go task as a baseline period. During the go task period, subjects are expected to press a button twice as often as in the go/no-go task period,

assuming that they perform the tasks appropriately. Due to the nature of go/no-go tasks, that go periods require increased response, we cannot fully equalize the motor loads of go and go/no-go periods. However, since motor effects are considered larger during the go period, we can expect that a go/no-go vs. go contrast would rule out motion artifacts. Accordingly, activation in a go/no-go task block is considered to reflect response inhibition and target detection, and is therefore more appropriate than a rest block as a baseline. Although fNIRS studies often use a paradigm where rest and task blocks were alternately performed (Herrmann et al., 2005), we suggest that it would be more suitable for studies using younger ADHD children to adopt experimental paradigms employing alternate go and go/no-go blocks, which have been commonly used in fMRI studies (Altshuler et al., 2005; Dillo et al., 2010; Ma et al., 2012; Vaidya et al., 1998).

5. Conclusion

In the current study exploring fNIRS-based diagnosis on the effects of MPH administration to ADHD children using a double-blind, placebo-controlled, cross-over design, we presented the following findings: 1) Relative to control subjects, unmedicated ADHD children exhibited reduced brain activation in the right IFG and MFG during go/no-go task blocks. 2) The reduced activation in the right inferior and middle frontal gyri was acutely normalized after MPH administration, but not after placebo administration. 3) Compared to the placebo-induced activation, the MPH-induced right IFG/MFG activation was significantly larger. These findings led us to conclude that the activation in the right inferior and middle frontal gyri could serve as an objective neuro-functional biomarker to indicate the effects of MPH on ADHD children. fNIRS-based examination on the effect of MPH was applicable to ADHD children as young as 6 years old. This promising technique will enable the early clinical diagnosis and treatment of ADHD children.

Acknowledgements

We appreciate ELCS for the English proofreading. We thank Illpop (http://illpop.com/animal_top01.htm) for kindly providing source pictures for the experimental materials. This work was supported in part by the Grant-in-Aid for Scientific Research from the Japan Society for Promotion of Science (22242012 to ID, 23390354 to EW, 23700885 to HD, 23650217 to ID, 80382951 to YM, and 70438662 to MN), and Health and Labor Sciences Research Grants, Research on Psychiatric and Neurological Diseases and Mental Health (to ID).

Appendix A. Supplementary data

Supplementary data to this article can be found online at http://dx.doi.org/10.1016/j.nicl.2012.10.001.

References

Altshuler, L.L., Bookheimer, S.Y., Townsend, J., Proenza, M.A., Eisenberger, N., Sabb, F., Mintz, J., Cohen, M.S., 2005. Blunted activation in orbitofrontal cortex during mania: a functional magnetic resonance imaging study. Biological Psychiatry 58, 763–769.

American Psychiatric Association, 1994. Diagnostic and Statistical Manual of Mental Disorders, 4th ed. American Psychiatric Association, Washington, DC.

Anderson, C.M., Polcari, A., Lowen, S.B., Renshaw, P.F., Teicher, M.H., 2002. Effects of methylphenidate on functional magnetic resonance relaxometry of the cerebellar vermis in boys with ADHD. The American Journal of Psychiatry 159, 1322–1328.

Arnsten, A.F., 2006. Stimulants: therapeutic actions in ADHD. Neuropsychopharmacology 31, 2376–2383.

Aron, A.R., Poldrack, R.A., 2005. The cognitive neuroscience of response inhibition: relevance for genetic research in attention-deficit/hyperactivity disorder. Biological Psychiatry 57, 1285–1292.

Aron, A.R., Dowson, J.H., Sahakian, B.J., Robbins, T.W., 2003. Methylphenidate improves response inhibition in adults with attention-deficit/hyperactivity disorder. Biological Psychiatry 54, 1465–1468.

Barkley, R.A., 1991. The ecological validity of laboratory and analogue assessment methods of ADHD symptoms. Journal of Abnormal Child Psychology 19, 149–178.

Beauregard, M., Levesque, J., 2006. Functional magnetic resonance imaging investigation of the effects of neurofeedback training on the neural bases of selective attention and response inhibition in children with attention-deficit/hyperactivity disorder. Applied Psychophysiology and Biofeedback 31, 3–20.

Bedard, A.C., Ickowicz, A., Logan, G.D., Hogg-Johnson, S., Schachar, R., Tannock, R., 2003. Selective inhibition in children with attention-deficit hyperactivity disorder off and on stimulant medication. Journal of Abnormal Child Psychology 31, 315–327.

Bedard, A.C., Schulz, K.P., Cook Jr., E.H., Fan, J., Clerkin, S.M., Ivanov, I., Halperin, J.M., Newcorn, J.H., 2010. Dopamine transporter gene variation modulates activation of striatum in youth with ADHD. NeuroImage 53, 935–942.

Biederman, J., Monuteaux, M.C., Spencer, T., Wilens, T.E., Faraone, S.V., 2009. Do stimulants protect against psychiatric disorders in youth with ADHD? A 10-year follow-up study. Pediatrics 124, 71–78.

Boecker, M., Buecheler, M.M., Schroeter, M.L., Gauggel, S., 2007. Prefrontal brain activation during stop-signal response inhibition: an event-related functional near-infrared spectroscopy study. Behavioural Brain Research 176, 259–266.

Booth, J.R., Burman, D.D., Meyer, J.R., Lei, Z., Trommer, B.L., Davenport, N.D., Li, W., Parrish, T.B., Gitelman, D.R., Mesulam, M.M., 2005. Larger deficits in brain networks for response inhibition than for visual selective attention in attention deficit hyperactivity disorder (ADHD). Journal of Child Psychology and Psychiatry 46, 94–111.

Buchsbaum, B.R., Greer, S., Chang, W.L., Berman, K.F., 2005. Meta-analysis of neuroimaging studies of the Wisconsin card-sorting task and component processes. Human Brain Mapping 25, 35–45.

Chabernaud, C., Mennes, M., Kelly, C., Nooner, K., Di Martino, A., Castellanos, F.X., Milham, M.P., 2012. Dimensional brain–behavior relationships in children with attention-deficit/hyperactivity disorder. Biological Psychiatry 71, 434–442.

Cope, M., Delpy, D.T., Reynolds, E.O., Wray, S., Wyatt, J., van der Zee, P., 1988. Methods of quantitating cerebral near infrared spectroscopy data. Advances in Experimental Medicine and Biology 222, 183–189.

Cui, X., Bray, S., Bryant, D.M., Glover, G.H., Reiss, A.L., 2011. A quantitative comparison of NIRS and fMRI across multiple cognitive tasks. NeuroImage 54, 2808–2821.

de Zeeuw, P., Schnack, H.G., van Belle, J., Weusten, J., van Dijk, S., Langen, M., Brouwer, R.M., van Engeland, H., Durston, S., 2012. Differential brain development with low and high IQ in attention-deficit/hyperactivity disorder. PLoS One 7, e35770.

Dennis, M., Francis, D.J., Cirino, P.T., Schachar, R., Barnes, M.A., Fletcher, J.M., 2009. Why IQ is not a covariate in cognitive studies of neurodevelopmental disorders. Journal of the International Neuropsychological Society 15, 331–343.

Derefinko, K.J., Adams, Z.W., Milich, R., Fillmore, M.T., Lorch, E.P., Lynam, D.R., 2008. Response style differences in the inattentive and combined subtypes of attention-deficit/hyperactivity disorder. Journal of Abnormal Child Psychology 36, 745–758.

Dibbets, P., Evers, L., Hurks, P., Marchetta, N., Jolles, J., 2009. Differences in feedback- and inhibition-related neural activity in adult ADHD. Brain and Cognition 70, 73–83.

Dillo, W., Goke, A., Prox-Vagedes, V., Szycik, G.R., Roy, M., Donnerstag, F., Emrich, H.M., Ohlmeier, M.D., 2010. Neuronal correlates of ADHD in adults with evidence for compensation strategies—a functional MRI study with a Go/No-Go paradigm. German Medical Science 8, Doc09.

Dittmann, R.W., Wehmeier, P.M., Schacht, A., Minarzyk, A., Lehmann, M., Sevecke, K., Lehmkuhl, G., 2009. Atomoxetine treatment and ADHD-related difficulties as assessed by adolescent patients, their parents and physicians. Child and Adolescent Psychiatry and Mental Health 3, 21.

Drechsler, R., Brandeis, D., Foldenyi, M., Imhof, K., Steinhausen, H.C., 2005. The course of neuropsychological functions in children with attention deficit hyperactivity disorder from late childhood to early adolescence. Journal of Child Psychology and Psychiatry 46, 824–836.

Durston, S., Thomas, K.M., Worden, M.S., Yang, Y., Casey, B.J., 2002. The effect of preceding context on inhibition: an event-related fMRI study. NeuroImage 16, 449–453.

Durston, S., Tottenham, N.T., Thomas, K.M., Davidson, M.C., Eigsti, I.M., Yang, Y., Ulug, A.M., Casey, B.J., 2003. Differential patterns of striatal activation in young children with and without ADHD. Biological Psychiatry 53, 871–878.

Durston, S., Hulshoff Pol, H.E., Schnack, H.G., Buitelaar, J.K., Steenhuis, M.P., Minderaa, R.B., Kahn, R.S., van Engeland, H., 2004. Magnetic resonance imaging of boys with attention-deficit/hyperactivity disorder and their unaffected siblings. Journal of the American Academy of Child and Adolescent Psychiatry 43, 332–340.

Durston, S., Davidson, M.C., Mulder, M.J., Spicer, J.A., Galvan, A., Tottenham, N., Scheres, A., Xavier Castellanos, F., van Engeland, H., Casey, B.J., 2007. Neural and behavioral correlates of expectancy violations in attention-deficit hyperactivity disorder. Journal of Child Psychology and Psychiatry 48, 881–889.

Ehlis, A.C., Bahne, C.G., Jacob, C.P., Herrmann, M.J., Fallgatter, A.J., 2008. Reduced lateral prefrontal activation in adult patients with attention-deficit/hyperactivity disorder (ADHD) during a working memory task: a functional near-infrared spectroscopy (fNIRS) study. Journal of Psychiatric Research 42, 1060–1067.

Eliassen, J.C., Souza, T., Sanes, J.N., 2001. Human brain activation accompanying explicitly directed movement sequence learning. Experimental Brain Research 141, 269–280.

Epstein, J.N., Casey, B.J., Tonev, S.T., Davidson, M., Reiss, A.L., Garrett, A., Hinshaw, S.P., Greenhill, L.L., Vitolo, A., Kotler, L.A., Jarrett, M.A., Spicer, J., 2007. Assessment and prevention of head motion during imaging of patients with attention deficit hyperactivity disorder. Psychiatry Research 155, 75–82.

Fair, D.A., Posner, J., Nagel, B.J., Bathula, D., Dias, T.G., Mills, K.L., Blythe, M.S., Giwa, A., Schmitt, C.F., Nigg, J.T., 2010. Atypical default network connectivity in youth with attention-deficit/hyperactivity disorder. Biological Psychiatry 68, 1084–1091.

Fischer, H., Wright, C.I., Whalen, P.J., McInerney, S.C., Shin, L.M., Rauch, S.L., 2003. Brain habituation during repeated exposure to fearful and neutral faces: a functional MRI study. Brain Research Bulletin 59, 387–392.

Frazier, T.W., Demaree, H.A., Youngstrom, E.A., 2004. Meta-analysis of intellectual and neuropsychological test performance in attention-deficit/hyperactivity disorder. Neuropsychology 18, 543–555.
Garavan, H., Ross, T.J., Stein, E.A., 1999. Right hemispheric dominance of inhibitory control: an event-related functional MRI study. Proceedings of the National Academy of Sciences of the United States of America 96, 8301–8306.
Garavan, H., Ross, T.J., Murphy, K., Roche, R.A., Stein, E.A., 2002. Dissociable executive functions in the dynamic control of behavior: inhibition, error detection, and correction. NeuroImage 17, 1820–1829.
Garavan, H., Ross, T.J., Kaufman, J., Stein, E.A., 2003. A midline dissociation between error-processing and response-conflict monitoring. NeuroImage 20, 1132–1139.
Garavan, H., Hester, R., Murphy, K., Fassbender, C., Kelly, C., 2006. Individual differences in the functional neuroanatomy of inhibitory control. Brain Research 1105, 130–142.
Grafton, S.T., Mazziotta, J.C., Woods, R.P., Phelps, M.E., 1992. Human functional anatomy of visually guided finger movements. Brain 115 (Pt 2), 565–587.
Herrmann, M.J., Ehlis, A.C., Fallgatter, A.J., 2004. Bilaterally reduced frontal activation during a verbal fluency task in depressed patients as measured by near-infrared spectroscopy. The Journal of Neuropsychiatry and Clinical Neurosciences 16, 170–175.
Herrmann, M.J., Plichta, M.M., Ehlis, A.C., Fallgatter, A.J., 2005. Optical topography during a Go–NoGo task assessed with multi-channel near-infrared spectroscopy. Behavioural Brain Research 160, 135–140.
Hester, R.L., Murphy, K., Foxe, J.J., Foxe, D.M., Javitt, D.C., Garavan, H., 2004. Predicting success: patterns of cortical activation and deactivation prior to response inhibition. Journal of Cognitive Neuroscience 16, 776–785.
Hock, C., Villringer, K., Müller-Spahn, F., Wenzel, R., Heekeren, H., Schuh-Hofer, S., Hofmann, M., Minoshima, S., Schwaiger, M., Dirnagl, U., Villringer, A., 1997. Decrease in parietal cerebral hemoglobin oxygenation during performance of a verbal fluency task in patients with Alzheimer's disease monitored by means of near-infrared spectroscopy (NIRS) — correlation with simultaneous rCBF-PET measurements. Brain Research 755, 293–303.
Inoue, Y., Sakihara, K., Gunji, A., Ozawa, H., Kimiya, S., Shinoda, H., Kaga, M., Inagaki, M., 2012. Reduced prefrontal hemodynamic response in children with ADHD during the go/nogo task: a NIRS study. Neuroreport 23, 55–60.
Jourdan Moser, S., Cutini, S., Weber, P., Schroeter, M.L., 2009. Right prefrontal brain activation due to Stroop interference is altered in attention-deficit hyperactivity disorder — a functional near-infrared spectroscopy study. Psychiatry Research 173, 190–195.
Jurcak, V., Tsuzuki, D., Dan, I., 2007. 10/20, 10/10, and 10/5 systems revisited: their validity as relative head-surface-based positioning systems. NeuroImage 34, 1600–1611.
Karch, S., Thalmeier, T., Lutz, J., Cerovecki, A., Opgen-Rhein, M., Hock, B., Leicht, G., Hennig-Fast, K., Meindl, T., Riedel, M., Mulert, C., Pogarell, O., 2010. Neural correlates (ERP/fMRI) of voluntary selection in adult ADHD patients. European Archives of Psychiatry and Clinical Neuroscience 260, 427–440.
Kiehl, K.A., Liddle, P.F., 2003. Reproducibility of the hemodynamic response to auditory oddball stimuli: a six-week test–retest study. Human Brain Mapping 18, 42–52.
Konishi, S., Nakajima, K., Uchida, I., Kikyo, H., Kameyama, M., Miyashita, Y., 1999. Common inhibitory mechanism in human inferior prefrontal cortex revealed by event-related functional MRI. Brain 122 (Pt 5), 981–991.
Kuntsi, J., Eley, T.C., Taylor, A., Hughes, C., Asherson, P., Caspi, A., Moffitt, T.E., 2004. Co-occurrence of ADHD and low IQ has genetic origins. American Journal of Medical Genetics. Part B, Neuropsychiatric Genetics 124B, 41–47.
Langenecker, S.A., Nielson, K.A., 2003. Frontal recruitment during response inhibition in older adults replicated with fMRI. NeuroImage 20, 1384–1392.
Law, I., Svarer, C., Holm, S., Paulson, O.B., 1997. The activation pattern in normal humans during suppression, imagination and performance of saccadic eye movements. Acta Physiologica Scandinavica 161, 419–434.
Liddle, P.F., Kiehl, K.A., Smith, A.M., 2001. Event-related fMRI study of response inhibition. Human Brain Mapping 12, 100–109.
Loubinoux, I., Carel, C., Alary, F., Boulanouar, K., Viallard, G., Manelfe, C., Rascol, O., Celsis, P., Chollet, F., 2001. Within-session and between-session reproducibility of cerebral sensorimotor activation: a test–retest effect evidenced with functional magnetic resonance imaging. Journal of Cerebral Blood Flow and Metabolism 21, 592–607.
Ma, J., Lei, D., Jin, X., Du, X., Jiang, F., Li, F., Zhang, Y., Shen, X., 2012. Compensatory brain activation in children with attention deficit/hyperactivity disorder during a simplified go/no-go task. Journal of Neural Transmission 119, 613–619.
Maki, A., Yamashita, Y., Ito, Y., Watanabe, E., Mayanagi, Y., Koizumi, H., 1995. Spatial and temporal analysis of human motor activity using noninvasive NIR topography. Medical Physics 22, 1997–2005.
Matsuo, K., Kato, T., Fukuda, M., Kato, N., 2000. Alteration of hemoglobin oxygenation in the frontal region in elderly depressed patients as measured by near-infrared spectroscopy. The Journal of Neuropsychiatry and Clinical Neurosciences 12, 465–471.
Matsuo, K., Taneichi, K., Matsumoto, A., Ohtani, T., Yamasue, H., Sakano, Y., Sasaki, T., Sadamatsu, M., Kasai, K., Iwanami, A., Asukai, N., Kato, N., Kato, T., 2003. Hypoactivation of the prefrontal cortex during verbal fluency test in PTSD: a near-infrared spectroscopy study. Psychiatry Research 124, 1–10.
Menon, V., Adleman, N.E., White, C.D., Glover, G.H., Reiss, A.L., 2001. Error-related brain activation during a go/nogo response inhibition task. Human Brain Mapping 12, 131–143.
Monden, Y., Dan, H., Nagashima, M., Dan, I., Kyutoku, Y., Okamoto, M., Yamagata, T., Momoi, M.Y., Watanabe, E., 2012. Clinically-oriented monitoring of acute effects of methylphenidate on cerebral hemodynamics in ADHD children using fNIRS. Clinical Neurophysiology 123, 1147–1157.
Moriai-Izawa, A., Dan, H., Dan, I., Sano, T., Oguro, K., Yokota, H., Tsuzuki, D., Watanabe, E., 2012. Multichannel fNIRS assessment of overt and covert confrontation naming. Brain and Language 121, 185–193.
Mostofsky, S.H., Simmonds, D.J., 2008. Response inhibition and response selection: two sides of the same coin. Journal of Cognitive Neuroscience 20, 751–761.
Mostofsky, S.H., Schafer, J.G., Abrams, M.T., Goldberg, M.C., Flower, A.A., Boyce, A., Courtney, S.M., Calhoun, V.D., Kraut, M.A., Denckla, M.B., Pekar, J.J., 2003. fMRI evidence that the neural basis of response inhibition is task-dependent. Brain Research. Cognitive Brain Research 17, 419–430.
Mulligan, R.C., Knopik, V.S., Sweet, L.H., Fischer, M., Seidenberg, M., Rao, S.M., 2011. Neural correlates of inhibitory control in adult attention deficit/hyperactivity disorder: evidence from the Milwaukee longitudinal sample. Psychiatry Research 194, 119–129.
Negoro, H., Sawada, M., Iida, J., Ota, T., Tanaka, S., Kishimoto, T., 2010. Prefrontal dysfunction in attention-deficit/hyperactivity disorder as measured by near-infrared spectroscopy. Child Psychiatry and Human Development 41, 193–203.
Newcorn, J.H., Halperin, J.M., Jensen, P.S., Abikoff, H.B., Arnold, L.E., Cantwell, D.P., Conners, C.K., Elliott, G.R., Epstein, J.N., Greenhill, L.L., Hechtman, L., Hinshaw, S.P., Hoza, B., Kraemer, H.C., Pelham, W.E., Severe, J.B., Swanson, J.M., Wells, K.C., Wigal, T., Vitiello, B., 2001. Symptom profiles in children with ADHD: effects of comorbidity and gender. Journal of the American Academy of Child and Adolescent Psychiatry 40, 137–146.
Okamoto, M., Dan, I., 2005. Automated cortical projection of head-surface locations for transcranial functional brain mapping. NeuroImage 26, 18–28.
Okamoto, M., Dan, H., Sakamoto, K., Takeo, K., Shimizu, K., Kohno, S., Oda, I., Isobe, S., Suzuki, T., Kohyama, K., Dan, I., 2004a. Three-dimensional probabilistic anatomical cranio-cerebral correlation via the international 10–20 system oriented for transcranial functional brain mapping. NeuroImage 21, 99–111.
Okamoto, M., Dan, H., Shimizu, K., Takeo, K., Amita, T., Oda, I., Konishi, I., Sakamoto, K., Isobe, S., Suzuki, T., Kohyama, K., Dan, I., 2004b. Multimodal assessment of cortical activation during apple peeling by NIRS and fMRI. NeuroImage 21, 1275–1288.
Okamoto, M., Matsunami, M., Dan, H., Kohata, T., Kohyama, K., Dan, I., 2006. Prefrontal activity during taste encoding: an fNIRS study. NeuroImage 31, 796–806.
Peterson, B.S., Potenza, M.N., Wang, Z., Zhu, H., Martin, A., Marsh, R., Plessen, K.J., Yu, S., 2009. An FMRI study of the effects of psychostimulants on default-mode processing during Stroop task performance in youths with ADHD. The American Journal of Psychiatry 166, 1286–1294.
Pietrzak, R.H., Mollica, C.M., Maruff, P., Snyder, P.J., 2006. Cognitive effects of immediate-release methylphenidate in children with attention-deficit/hyperactivity disorder. Neuroscience and Biobehavioral Reviews 30, 1225–1245.
Rorden, C., Brett, M., 2000. Stereotaxic display of brain lesions. Behavioural Neurology 12, 191–200.
Rubia, K., Overmeyer, S., Taylor, E., Brammer, M., Williams, S.C., Simmons, A., Bullmore, E.T., 1999. Hypofrontality in attention deficit hyperactivity disorder during higher-order motor control: a study with functional MRI. The American Journal of Psychiatry 156, 891–896.
Rubia, K., Russell, T., Overmeyer, S., Brammer, M.J., Bullmore, E.T., Sharma, T., Simmons, A., Williams, S.C., Giampietro, V., Andrew, C.M., Taylor, E., 2001. Mapping motor inhibition: conjunctive brain activations across different versions of go/no-go and stop tasks. NeuroImage 13, 250–261.
Rubia, K., Smith, A.B., Brammer, M.J., Taylor, E., 2003. Right inferior prefrontal cortex mediates response inhibition while mesial prefrontal cortex is responsible for error detection. NeuroImage 20, 351–358.
Rubia, K., Smith, A.B., Brammer, M.J., Toone, B., Taylor, E., 2005. Abnormal brain activation during inhibition and error detection in medication-naive adolescents with ADHD. The American Journal of Psychiatry 162, 1067–1075.
Rubia, K., Halari, R., Cubillo, A., Mohammad, A.M., Brammer, M., Taylor, E., 2009. Methylphenidate normalises activation and functional connectivity deficits in attention and motivation networks in medication-naive children with ADHD during a rewarded continuous performance task. Neuropharmacology 57, 640–652.
Sakatani, K., Lichty, W., Xie, Y., Li, S., Zuo, H., 1999. Effects of aging on language-activated cerebral blood oxygenation changes of the left prefrontal cortex: Near infrared spectroscopy study. Journal of Stroke and Cerebrovascular Diseases 8, 398–403.
Schecklmann, M., Ehlis, A.C., Plichta, M.M., Romanos, J., Heine, M., Boreatti-Hummer, A., Jacob, C., Fallgatter, A.J., 2008. Diminished prefrontal oxygenation with normal and above-average verbal fluency performance in adult ADHD. Journal of Psychiatric Research 43, 98–106.
Schecklmann, M., Romanos, M., Bretscher, F., Plichta, M.M., Warnke, A., Fallgatter, A.J., 2010. Prefrontal oxygenation during working memory in ADHD. Journal of Psychiatric Research 44, 621–628.
Schulz, K.P., Fan, J., Tang, C.Y., Newcorn, J.H., Buchsbaum, M.S., Cheung, A.M., Halperin, J.M., 2004. Response inhibition in adolescents diagnosed with attention deficit hyperactivity disorder during childhood: an event-related FMRI study. The American Journal of Psychiatry 161, 1650–1657.
Sebastian, A., Gerdes, B., Feige, B., Kloppel, S., Lange, T., Philipsen, A., Tebartz van Elst, L., Lieb, K., Tuscher, O., 2012. Neural correlates of interference inhibition, action withholding and action cancelation in adult ADHD. Psychiatry Research 202, 132–141.
Shattuck, D.W., Mirza, M., Adisetiyo, V., Hojatkashani, C., Salamon, G., Narr, K.L., Poldrack, R.A., Bilder, R.M., Toga, A.W., 2008. Construction of a 3D probabilistic atlas of human cortical structures. NeuroImage 39, 1064–1080.
Shinba, T., Nagano, M., Kariya, N., Ogawa, K., Shinozaki, T., Shimosato, S., Hoshi, Y., 2004. Near-infrared spectroscopy analysis of frontal lobe dysfunction in schizophrenia. Biological Psychiatry 55, 154–164.
Simmonds, D.J., Pekar, J.J., Mostofsky, S.H., 2008. Meta-analysis of go/no-go tasks demonstrating that fMRI activation associated with response inhibition is task-dependent. Neuropsychologia 46, 224–232.

Singh, A.K., Okamoto, M., Dan, H., Jurcak, V., Dan, I., 2005. Spatial registration of multichannel multi-subject fNIRS data to MNI space without MRI. NeuroImage 27, 842–851.
Siniatchkin, M., Glatthaar, N., von Muller, G.G., Prehn-Kristensen, A., Wolff, S., Knochel, S., Steinmann, E., Sotnikova, A., Stephani, U., Petermann, F., Gerber, W.D., 2012. Behavioural treatment increases activity in the cognitive neuronal networks in children with attention deficit/hyperactivity disorder. Brain Topography 25, 332–344.
Slifer, K.J., Koontz, K.L., Cataldo, M.F., 2002. Operant-contingency-based preparation of children for functional magnetic resonance imaging. Journal of Applied Behavior Analysis 35, 191–194.
Smith, A.B., Taylor, E., Brammer, M., Toone, B., Rubia, K., 2006. Task-specific hypoactivation in prefrontal and temporoparietal brain regions during motor inhibition and task switching in medication-naive children and adolescents with attention deficit hyperactivity disorder. The American Journal of Psychiatry 163, 1044–1051.
Solanto, M.V., Schulz, K.P., Fan, J., Tang, C.Y., Newcorn, J.H., 2009. Event-related FMRI of inhibitory control in the predominantly inattentive and combined subtypes of ADHD. Journal of Neuroimaging 19, 205–212.
Spencer, T.J., 2004. ADHD treatment across the life cycle. The Journal of Clinical Psychiatry 65 (Suppl. 3), 22–26.
Strangman, G., Boas, D.A., Sutton, J.P., 2002. Non-invasive neuroimaging using near-infrared light. Biological Psychiatry 52, 679–693.
Suto, T., Fukuda, M., Ito, M., Uehara, T., Mikuni, M., 2004. Multichannel near-infrared spectroscopy in depression and schizophrenia: cognitive brain activation study. Biological Psychiatry 55, 501–511.
Tamm, L., Menon, V., Ringel, J., Reiss, A.L., 2004. Event-related fMRI evidence of frontotemporal involvement in aberrant response inhibition and task switching in attention-deficit/hyperactivity disorder. Journal of the American Academy of Child and Adolescent Psychiatry 43, 1430–1440.
Tannock, R., Schachar, R., Logan, G., 1995. Methylphenidate and cognitive flexibility: dissociated dose effects in hyperactive children. Journal of Abnormal Child Psychology 23, 235–266.
Teicher, M.H., Anderson, C.M., Polcari, A., Glod, C.A., Maas, L.C., Renshaw, P.F., 2000. Functional deficits in basal ganglia of children with attention-deficit/hyperactivity disorder shown with functional magnetic resonance imaging relaxometry. Nature Medicine 6, 470–473.
Tsujii, T., Sakatani, K., Nakashima, E., Igarashi, T., Katayama, Y., 2011. Characterization of the acute effects of alcohol on asymmetry of inferior frontal cortex activity during a go/no-go task using functional near-infrared spectroscopy. Psychopharmacology 217, 595–603.
Tsuzuki, D., Jurcak, V., Singh, A.K., Okamoto, M., Watanabe, E., Dan, I., 2007. Virtual spatial registration of stand-alone fNIRS data to MNI space. NeuroImage 34, 1506–1518.
Tsuzuki, D., Cai, D.S., Dan, H., Kyutoku, Y., Fujita, A., Watanabe, E., Dan, I., 2012. Stable and convenient spatial registration of stand-alone NIRS data through anchor-based probabilistic registration. Neuroscience Research 72, 163–171.
Vaidya, C.J., Austin, G., Kirkorian, G., Ridlehuber, H.W., Desmond, J.E., Glover, G.H., Gabrieli, J.D., 1998. Selective effects of methylphenidate in attention deficit hyperactivity disorder: a functional magnetic resonance study. Proceedings of the National Academy of Sciences of the United States of America 95, 14494–14499.
Vaidya, C.J., Bunge, S.A., Dudukovic, N.M., Zalecki, C.A., Elliott, G.R., Gabrieli, J.D., 2005. Altered neural substrates of cognitive control in childhood ADHD: evidence from functional magnetic resonance imaging. The American Journal of Psychiatry 162, 1605–1613.
Vasic, N., Plichta, M.M., Wolf, R.C., Fallgatter, A.J., Sosic-Vasic, Z., Gron, G., in press. Reduced neural error signaling in left inferior prefrontal cortex in young adults with ADHD. Journal of Attention Disorders.
Weber, P., Lutschg, J., Fahnenstich, H., 2005. Cerebral hemodynamic changes in response to an executive function task in children with attention-deficit hyperactivity disorder measured by near-infrared spectroscopy. Journal of Developmental and Behavioral Pediatrics 26, 105–111.
Wehmeier, P.M., Schacht, A., Wolff, C., Otto, W.R., Dittmann, R.W., Banaschewski, T., 2011. Neuropsychological outcomes across the day in children with attention-deficit/hyperactivity disorder treated with atomoxetine: results from a placebo-controlled study using a computer-based continuous performance test combined with an infra-red motion-tracking device. Journal of Child and Adolescent Psychopharmacology 21, 433–444.
Wilens, T.E., 2008. Effects of methylphenidate on the catecholaminergic system in attention-deficit/hyperactivity disorder. Journal of Clinical Psychopharmacology 28, S46–S53.
Yerys, B.E., Jankowski, K.F., Shook, D., Rosenberger, L.R., Barnes, K.A., Berl, M.M., Ritzl, E.K., Vanmeter, J., Vaidya, C.J., Gaillard, W.D., 2009. The fMRI success rate of children and adolescents: typical development, epilepsy, attention deficit/hyperactivity disorder, and autism spectrum disorders. Human Brain Mapping 30, 3426–3435.
Zhu, C.Z., Zang, Y.F., Cao, Q.J., Yan, C.G., He, Y., Jiang, T.Z., Sui, M.Q., Wang, Y.F., 2008. Fisher discriminative analysis of resting-state brain function for attention-deficit/hyperactivity disorder. NeuroImage 40, 110–120.

frontiers in PSYCHIATRY

ORIGINAL RESEARCH ARTICLE
published: 18 March 2013
doi: 10.3389/fpsyt.2013.00016

Gray matter changes in subjects at high risk for developing psychosis and first-episode schizophrenia: a voxel-based structural MRI study

Kazue Nakamura[1]*, Tsutomu Takahashi[1,2], Kiyotaka Nemoto[3], Atsushi Furuichi[1], Shimako Nishiyama[1], Yumiko Nakamura[1], Eiji Ikeda[1], Mikio Kido[1], Kyo Noguchi[4], Hikaru Seto[4] and Michio Suzuki[1,2]

[1] Department of Neuropsychiatry, Graduate School of Medicine and Pharmaceutical Sciences, University of Toyama, Toyama, Japan
[2] Core Research for Evolutional Science and Technology, Japan Science and Technology Corporation, Tokyo, Japan
[3] Department of Psychiatry, Graduate School of Comprehensive Human Sciences, University of Tsukuba, Tsukuba, Ibaraki, Japan
[4] Department of Radiology, Graduate School of Medicine and Pharmaceutical Sciences, University of Toyama, Toyama, Japan

Edited by:
Jun Soo Kwon, Seoul National University College of Medicine, South Korea

Reviewed by:
Stefan Borgwardt, University of Basel, Switzerland
Kim Jae-Jin, Yonsei University, South Korea

***Correspondence:**
Kazue Nakamura, Department of Neuropsychiatry, Graduate School of Medicine and Pharmaceutical Sciences, University of Toyama, 2630 Sugitani, Toyama 930-0194, Japan.
e-mail: krnaka@med.u-toyama.ac.jp

Objectives: The aim of the present study was to use a voxel-based magnetic resonance imaging method to investigate the neuroanatomical characteristics in subjects at high risk of developing psychosis compared with those of healthy controls and first-episode schizophrenia patients.

Methods: This study included 14 subjects with at-risk mental state (ARMS), 34 patients with first-episode schizophrenia, and 51 healthy controls. We used voxel-based morphometry with the Diffeomorphic Anatomical Registration through Exponentiated Lie Algebra tools to investigate the whole-brain difference in gray matter volume among the three groups.

Results: Compared with the healthy controls, the schizophrenia patients showed significant gray matter reduction in the left anterior cingulate gyrus. There was no significant difference in the gray matter volume between the ARMS and other groups.

Conclusion: The present study suggests that alteration of the anterior cingulate gyrus may be associated with development of frank psychosis. Further studies with a larger ARMS subjects would be required to examine the potential role of neuroimaging methods in the prediction of future transition into psychosis.

Keywords: schizophrenia, psychosis, high risk, MRI, cingulate gyrus

INTRODUCTION

Neuroimaging studies have demonstrated subtle but widespread brain structural alterations, such as volume reduction of fronto-temporo-limbic regions as well as enlarged lateral and third ventricles, in first-episode schizophrenia (Steen et al., 2006; Vita et al., 2006; Ellison-Wright et al., 2008), which are not due to illness chronicity and antipsychotic medication. Recent prospective longitudinal magnetic resonance imaging (MRI) studies, including our own data showing progressive gray matter reduction of the temporal region (approximately 2–3% per year) (Takahashi et al., 2010, 2011), further revealed progressive brain structural change and its relationship to clinical course or outcome in first-episode schizophrenia (Andreasen et al., 2011). These longitudinal findings might be consistent with the clinical observation that a long duration of untreated psychosis (DUP), which could lead to severe brain pathological changes during the early illness stage (Lappin et al., 2006; Takahashi et al., 2007), is related to poor outcome of schizophrenia patients (Marshall et al., 2005; Perkins et al., 2005). Examining potential neurobiological markers that predate the onset of psychosis might lead to appropriate early intervention and thus prevent deterioration of social function and the progression of structural brain alterations.

It is not yet clear at which illness stage brain abnormalities occur in schizophrenia. Subjects with at-risk mental state (ARMS), who exhibit prodromal-like symptoms and have an increased risk of developing psychosis (Yung et al., 2003), might share disease vulnerability as well as brain morphological changes with patients with overt schizophrenia. Subjects with ARMS are heterogeneous on the basis of their outcome, as only about 36% of them develop psychosis during 3-year follow-up (Fusar-Poli et al., 2012). Previous MRI studies using voxel-based morphometry (VBM), which allows automated whole-brain analysis, revealed more severe gray matter reduction predominantly in the fronto-temporo-limbic regions in ARMS subjects with later transition than in those without (Pantelis et al., 2003; Borgwardt et al., 2007; Fusar-Poli et al., 2011). More specifically, Fornito et al. (2008) revealed that baseline differences in the anterior cingulate cortical thickness distinguished between ARMS with and without later transition, but they did not directly compare ARMS subjects and patients with overt psychosis.

This voxel-based MRI study aimed to investigate the nature of neuroanatomical abnormalities in high-risk subjects compared with both healthy controls and first-episode schizophrenia patients. On the basis of previous neuroimaging findings, we predicted that both first-episode schizophrenia and ARMS subjects, especially those with later transition, would show brain morphological changes in fronto-temporo-limbic regions compared with healthy subjects.

MATERIALS AND METHODS

PARTICIPANTS

Fourteen individuals (10 males and 4 females) defined as ARMS for psychosis were recruited from the Consultation Support Service in Toyama (CAST), which was launched in 2006 as a specialized clinical setting to study and treat young persons (aged 15–30 years) at risk of developing psychosis (Mizuno et al., 2009). The subjects with ARMS were diagnosed according to the Comprehensive Assessment of ARMS (CAARMS) (Yung et al., 2004); they were characterized by one or more of the following: (1) attenuated psychotic symptoms; (2) brief, limited intermittent psychotic symptoms with spontaneous resolution; or (3) family history of psychosis in first-degree relatives or a personal history of schizotypal personality disorder accompanied by a decline in general functioning. Their clinical symptoms were assessed using the Scale for the Assessment of Negative Symptoms (SANS) (Andreasen, 1983) and the Scale for the Assessment of Positive Symptoms (SAPS) (Andreasen, 1984) at the time of scanning. Eleven ARMS subjects were neuroleptic-naïve at scanning, but two subjects were treated with atypical neuroleptics and one was receiving sulpiride. Their duration of medication use was shorter than 2 weeks for atypical neuroleptics and shorter than 6 months for sulpiride. They were also receiving benzodiazepines ($N = 2$), antidepressants ($N = 1$), and tandospirone ($N = 3$).

Thirty-four patients with first-episode schizophrenia (20 males and 14 females), who met the ICD-10 research criteria (World Health Organization, 1993), were recruited from the inpatient and outpatient clinics of the Department of Neuropsychiatry, Toyama University Hospital. The patients were diagnosed following structured clinical interviews by experienced psychiatrists using the Comprehensive Assessment of Symptoms and History (CASH; Andreasen et al., 1992). Their durations from manifestations of overt psychotic symptoms were shorter than 1 year. Their clinical symptoms were assessed using SANS and SAPS at the time of scanning. Thirty-three patients were receiving neuroleptic medication at the time of scanning; 2 patients were treated with typical neuroleptics, 26 were receiving atypical neuroleptics, 5 were taking both typical and atypical neuroleptics, and 1 patient was neuroleptic-free. They were also receiving anticholinergic drugs ($N = 8$), benzodiazepines ($N = 9$), antidepressants ($N = 1$), carbamazepine ($N = 1$), and lithium carbonate ($N = 3$).

Exclusion criteria for ARMS subjects and schizophrenia patients were other neurological diseases, past or present regular alcohol abuse, and/or consumption of illicit drugs as reported by the study participants and/or the patients' records, as well as past head trauma with loss of consciousness or electro-convulsive treatment.

The control subjects consisted of 51 healthy volunteers (30 males and 21 females) recruited from members of the community, hospital staff, and university students. They were given a questionnaire consisting of 15 items concerning their personal (13 items; including a history of obstetric complications, substantial head injury, seizures, neurological or psychiatric diseases, impaired thyroid function, hypertension, diabetes, and substance use) and family (2 items) histories of illness. They did not have any personal or family history of psychiatric illness in their first-degree relatives. This study was approved by the ethics committee of Toyama University. Written informed consent was obtained from all subjects prior to study participation.

MRI ACQUISITION

Magnetic resonance images were obtained by utilizing a 1.5-T Magnetom Vision (Siemens Medical System, Inc., Erlangen, Germany) with a three-dimensional gradient-echo sequence FLASH (fast low-angle shots) yielding 160–180 contiguous T1-weighted slices of 1.0-mm thickness in the sagittal plane. The imaging parameters were as follows: TR = 24 ms; TE = 5 ms; flip angle = 40°; field of view = 256 mm; and matrix size = 256 × 256 pixels. The voxel size was 1.0 mm × 1.0 mm × 1.0 mm. All scans in the patient and control groups were acquired in the same system with the same protocol.

MRI DATA PROCESSING

All T1-weighted MRI data were first converted from the Dicom format to the NIFTI format and then processed using Statistical Parametric Mapping 8 (SPM8, Wellcome Institute of Neurology, University College London, UK, http://www.fil.ion.ucl.ac.uk/spm) running under MATLAB R2008b (The MathWorks Inc., USA).

The unified segmentation model consisting of spatial normalization, bias field correction, and tissue segmentation was performed in order to improve the quality of data preprocessing (Ashburner and Friston, 2005). Tissue probability maps were registered to the subject's data, and final tissue probability maps were derived from prior maps with the use of a combination with tissue probabilities based on the voxel intensity. To make the processed data more accurate, we used the Diffeomorphic Anatomical Registration through Exponentiated Lie Algebra (DARTEL) (Ashburner, 2007; Ashburner and Friston, 2009; Klein et al., 2009) tool in SPM8. DARTEL is not integrated into the segmentation model and requires the input of gray matter tissue maps produced by unified segmentation. This algorithm records inter-subject images using diffeomorphisms, which preserve the object properties through deformations, twistings, and stretchings, and archives a more accurate inter-subject registration. Because DARTEL produces a more accurate registration, it improves the sensitivity of finding and localizing differences between groups in terms of the gray matter volume. Registered tissue maps were transformed to the stereotactic space of the Montreal Neurological Institute (MNI) and multiplied with the Jacobian determinants of the deformations in order to preserve the volume of tissue in each structure. Finally, the modulated, warped tissue maps were then written with an isotropic voxel resolution of 1.5 mm^3 and smoothed with a 10-mm Full-Width Half-Maximum (FWHM) Gaussian kernel (Salmond et al., 2002; Jones et al., 2005).

STATISTICAL ANALYSIS

Demographic data

Group differences in age, educational level, parental educational level, and intracranial volume (ICV) were examined with one-way analysis of variance (ANOVA) and *post hoc* Scheffé's test. Group differences in terms of gender were tested with Chi-square tests. The level of statistical significance was defined as $p < 0.05$ (two-tailed). Statistical analyses were performed with Statistica, version 06J for Windows (StatSoft Japan Inc., Tokyo, Japan).

Voxel-based analysis of gray matter volume

Gray matter volume differences between the ARMS subjects, schizophrenia patients, and healthy controls were analyzed using two-sample *t*-tests implemented in the general linear model approach of SPM8 with age and ICV as nuisance covariates. We used cluster level inference (the extent of contiguous clusters of individual significant voxels) for determination of statistical significance (Meisenzahl et al., 2008). Because cluster size distribution varies according to local smoothness, the cluster sizes in this study were adjusted according to the local smoothness within the framework of the Random Field Theory (RFT) (Worsley et al., 1999; Hayasaka et al., 2004). Our statistical inference was performed at the cluster level by assessing the SPM{t} images by the non-stationary cluster extent correction (Hayasaka et al., 2004), which has been reported to be robust when MRI experiments fulfill (1) degrees of freedom > 30 and (2) image smoothness (FWHM) > 3 × voxel sampling resolution (Hayasaka et al., 2004), as in this study. The cluster-defining threshold was set to $p < 0.001$. Then, a family-wise error-corrected (FWE) cluster size threshold of $p < 0.05$ was applied to account for multiple comparisons of the results (corrected cluster sizes). Finally, cluster sizes were adjusted for smoothness non-uniformity using the VBM8 toolbox (Gaser, 2009), which implements the methodology of Hayasaka et al. (2004).

Voxel coordinates are given as an indication of location in a standardized brain. Voxels were localized in MNI space and transformed into Talairach and Tournoux coordinates (Talairach and Tournoux, 1988).

RESULTS

DEMOGRAPHIC DATA

Table 1 shows demographic and clinical data of the subjects in this study. Groups were matched for gender, parental education, and ICV. However, the controls ($p < 0.001$) and schizophrenia patients ($p < 0.001$) were older than the ARMS subjects. The controls had a higher educational level than the other two groups ($p < 0.001$) and the schizophrenia patients had a higher educational level than the ARMS subjects ($p = 0.004$).

VOXEL-BASED ANALYSIS OF GRAY MATTER VOLUME

Compared with the healthy controls, the schizophrenia patients showed significant gray matter volume reduction in the left anterior cingulate gyrus (FWE-corrected $p = 0.047$) (**Figures 1** and **2**; **Table 2**). There was no difference between the ARMS subjects and the schizophrenia patients or the healthy controls.

DISCUSSION

In this study, we performed VBM analyses using the DARTEL method to investigate gray matter change in early psychosis. In comparison to the healthy controls, first-episode schizophrenia patients showed significant gray matter reduction in the left anterior cingulate gyrus, but the ARMS subjects showed no significant difference in gray matter volume. This negative finding may be partly related to the heterogeneity of the ARMS subjects, as those with later transition to psychosis had a similar distribution of the cingulate gyrus gray matter volume to that in first-episode schizophrenia patients (**Figure 2**). These preliminary results are partly consistent with previous findings by Fornito et al. (2008), who reported that baseline differences of anterior cingulate gyrus distinguish between high-risk individuals who do and do not subsequently develop overt psychosis.

Neuroimaging studies comparing schizophrenia patients to healthy controls have shown evidence of morphological change in the anterior cingulate gyrus (Ellison-Wright et al., 2008; Shepherd et al., 2012). Gray matter volume reduction (Salgado-Pineda et al., 2003; Koo et al., 2008; Meisenzahl et al., 2008; Leung et al., 2011) and reduced cortical thickness (Schultz et al., 2010) in the anterior

Table 1 | Clinical and demographic characteristics[a].

Characteristic	ARMS (*N* = 14)	Schizophrenia (*N* = 34)	Healthy control (*N* = 51)
Gender (male/female)	10/4	20/14	30/21
Age (years)[b]	18.9 (1.4)	24.7 (5.5)	23.9 (1.8)
Educational level (years)[c]	11.6 (1.4)	13.5 (2.0)	16.0 (1.7)
Parental educational level (years)	13.7 (1.4)	13.3 (1.7)	14.1 (2.2)
Age at onset (years)	N/A	23.3 (5.4)	N/A
Duration of medication (months)	0.43 (1.6)	1.7 (1.8)	N/A
Drug (mg/day, haloperidol equivalent)[d]	0.55 (1.1)	6.3 (6.5)	N/A
Intracranial volume (cm^3)	1557.8 (130.0)	1602.1 (150.7)	1573.6 (143.0)

[a] *Values given as mean (SD).*

[b] *Significant difference between groups.*

[c] *Significant difference between groups.*

[d] *The different typical and atypical neuroleptic dosages were converted into haloperidol equivalents using the guidelines of Toru (2001).*